Advances in Water Resources 62 (2013) 409–430

Contents lists available at SciVerse ScienceDirect

Advances in Water Resources

journal homepage: www.elsevier.com/locate/advwatres

A robust and efficient numerical method for multiphase equilibrium calculations: Application to CO_2–brine–rock systems at high temperatures, pressures and salinities

Allan M.M. Leal [a,*], Martin J. Blunt [a], Tara C. LaForce [b]

[a] Imperial College London, Qatar Carbonates and Carbon Storage Research Centre and Department of Earth Science and Engineering, London, UK
[b] CSIRO, Earth Science and Resource Engineering, Australia

ARTICLE INFO

Article history:
Available online 28 February 2013

Keywords:
Chemical equilibrium
Geochemistry
Multiphase system
Carbon storage

ABSTRACT

We present a robust and efficient method for calculating chemical equilibria of general multiphase systems. The method is based on a stoichiometric approach, which uses Newton's method to solve a system of mass-action equations coupled with a system of equilibrium constraints. A stabilisation procedure is developed to promote convergence of the calculation when a presupposed phase in the chemical system is absent in the equilibrium state. The formulation of the chemical equilibrium problem is developed by presuming no specific details of the involved phases and species. As a consequence, the method is flexible and general enough so that the calculation can be customised with a combination of thermodynamic models that are appropriate for the problem of interest. Finally, we show the use of the method to solve relevant geochemical equilibrium problems for modelling carbon storage in highly saline aquifers.

1. Introduction

Multiphase systems are encountered in numerous natural and industrial processes. The ability to model their chemical and physical behaviour is of utmost importance for many applications such as petroleum reservoir simulation, geochemical analyses of water–gas–rock systems, and design of carbon dioxide storage in geologic formations. However, accurate and comprehensive modelling of such systems is difficult and computationally expensive.

In this work we develop a numerical method for the thermodynamic equilibrium calculation of multiphase systems. Unlike the traditional approach of imposing only mass-balance conditions on the chemical elements of the system, the approach presented here permits the specification of other types of equilibrium constraints such as fixed activity or fugacity of a species, fixed partial pressure of a gas, fixed concentration or amount of a species, and others. This generality in specifying equilibrium constraints is important, for example, if the pH of an aqueous solution is known, or if the dissolution of a mineral needs to be analysed over a range of concentrations of aqueous carbon dioxide.

The formulation of the method assumes no specific details about the species and phases involved. Therefore, the method is generally applicable, allowing it to be used with any combination of phases and species. Such generality is achieved by representing thermodynamic quantities such as activity and its derivatives, chemical potentials, and equilibrium constants as abstract functions of temperature, pressure and composition. Therefore, the algorithm can be easily customised to allow the use of a combination of thermodynamic models for the problem of interest.

1.1. Existing geochemical solvers

In Smith and Missen [1], algorithms for chemical equilibrium calculation are classified in two types: one based on the *stoichiometric formulation*, and the other on the *nonstoichiometric formulation*. The former takes into account the stoichiometry among the species, which gives rise to a system of equilibrium reactions mathematically modelled by a system of non-linear mass-action equations. The latter, however, does not consider such stoichiometry and requires a minimisation of the Gibbs free energy of the system in order to determine its thermodynamic equilibrium state.

In this work we adopt a stoichiometric formulation for the derivation of the numerical method. This decision is made because the stoichiometric formulation requires fewer unknowns than its non-stoichiometric counterpart, which has its number of unknowns increased by the use of Lagrange multipliers. It should be remarked, however, that both formulations are mathematically equivalent as shown by Zeleznik and Gordon [2], and Van Zeggeren and Storey [3]. An alternative demonstration of this is shown in Appendix A.

* Corresponding author.
E-mail addresses: al2010@imperial.ac.uk (A.M.M. Leal), m.blunt@imperial.ac.uk (M.J. Blunt), tara.laforce@csiro.au (T.C. LaForce).

0309-1708
http://dx.doi.org/10.1016/j.advwatres.2013.02.006

Several geochemical solvers for equilibrium calculation exist in the literature. Commonly used computational packages for geochemistry modelling include MINEQL [4], MINEQL+ [5], WATEQ [6], WATEQ4F [7], MINTEQA2 [8], EQ3/6 [9], PHREEQC [10,11], CHESS [12], and Geochemist's Workbench [13], to name just a few. All these solvers are based on the stoichiometric formulation. Geochemical packages based on the nonstoichiometric formulation that use minimisation techniques for equilibrium calculations include GEM-Selektor [14], FactSage [15,16] and ChemSage [17].

Geochemical solvers typically assume numerous details about the species, reactions, and phases in a thermodynamic equilibrium calculation. These details can be, for example, an arbitrary decision to neglect the reactive consumption/production of water [8], the assumption that an aqueous phase always exists [8,10,13], or the assumption that a gaseous phase exists only under the imposition of a specified partial pressure/fugacity of a gaseous species [9,13,18,19].

The disadvantages that follow from assuming specific characteristics and models for the species, reactions, and phases are many. Firstly, handling so many particular and arbitrary cases can result in code bloat, which reduces efficiency and maintainability of the software. Secondly, it becomes complicated to add new features to the solver, since the introduction of new thermodynamic models and phase types might incur in several modifications throughout the code. Finally, restricting specific thermodynamic models for some types of species restricts the solver flexibility and applicability, preventing it from performing customised computations using the plethora of models existent in the literature.

Another common problem among some traditional geochemical solvers concerns the numerical techniques they use for solving the equilibrium equations. For instance, MINTEQA2 [8], EQ3/6 [9], PHREEQC [10,11], CHESS [12], and Geochemist's Workbench [13] use an incomplete Newton approach to solve the resulting system of non-linear equations. This incomplete Newton scheme can be traced back to Morel and Morgan [20] in their proposal of an algorithm for solving aqueous speciation. The approach consists of arranging the species in two disjoint sets: a set of basis (or master/component) species, and another of secondary species. Then, the composition of the basis species are calculated via Newton's method applied to the modified mass-balance equations, and the composition of the secondary species are calculated via a successive substitution approach using the mass-action equations.

The argument for this numerical scheme is to have a Jacobian matrix with reduced dimensions. As a result, less computational effort is spent in inverting matrices. However, calculating chemical equilibria with an incomplete Jacobian matrix is not necessarily faster than it would be with a complete Jacobian. This is because more iterations might be required for the former approach, since the quadratic convergence rate of Newton's method near the solution is no longer guaranteed. Moreover, one should note that the computational cost of evaluating complex equations of state and thermodynamic functions can be greater than that of inverting a complete Jacobian matrix.

Therefore, the numerical technique presented in this work uses a full Newton's method, as opposed to the incomplete approach discussed above. This guarantees an optimal convergence rate of the root-finding algorithm when the iterate is near the solution, even for highly non-linear multiphase systems.

An improvement of the numerical technique developed by Morel and Morgan [20] can be found in the work of Reed [21] for heterogeneous chemical equilibrium calculations involving minerals, gases and aqueous species. However, its methodology has some of the drawbacks discussed previously, such as the assumption of specific details about the system and the use of an incomplete Newton method. The method, for instance, would have difficulties modelling the full evaporation of an aqueous phase, since this phase is considered to always exist. Moreover, the handling of mineral phase appearance or disappearance at equilibrium is not performed by a general approach that could be applied to any phase. This is because the concept of mineral saturation is used to determine which mineral should be excluded or added to the calculation.

A recent work on multiphase geochemical speciation calculation can be found in Perez et al. [22]. The numerical method consists of combining two-phase flash calculations with aqueous speciation, where two independent routines that communicate with each other are used to solve the multiphase equilibrium problem. This differs from the methodology presented in this work, which solves the full equilibrium problem without making separate flash calculations to account for a gaseous phase.

1.2. Applications to carbon storage

Chemical equilibrium calculations for multiphase systems are of vital importance for modelling carbon storage in deep saline aquifers. Once CO_2 is injected underground, most of it may dissolve in brine, causing several relevant geochemical phenomena that affect its overall trapping. Therefore, in order to determine the fate of the injected CO_2, reactive porous media flow simulations are required, as evidenced, for example, by Johnson et al. [23], Lagneau et al. [24], Audigane et al. [25,26] and Fan et al. [27]. These simulations depend on tools capable of calculating the partitioning of the components among the phases as well as determining all local equilibrium phases.

As discussed above, many geochemical processes begin once CO_2 is dissolved. These include, for example, the acidification of the resident brine, which increases the significance of the reactions between aqueous species and primary minerals in the porous rock, Gunter et al. [28]. Moreover, secondary carbonate minerals can precipitate because of the water–rock interactions, indirectly sequestering CO_2 for geological times.

In this work we apply our multiphase equilibrium method to model certain problems related to CO_2 sequestration in saline aquifers. These include the numerical investigation of the solubility of carbon dioxide in brines and the calculation of phase behaviour in systems composed of aqueous, gaseous and mineral phases.

The brines assumed for the calculation of CO_2 solubility are those derived from the salts: NaCl, NaCl + KCl, $MgCl_2$, and $CaCl_2$. Comparison of the calculations with experimental data is done using the recent measurements of Tong et al. [29] and Hou et al. [30] at high temperatures, pressures and brine salinities. A combination of activity and fugacity coefficient models is used for species CO_2(aq) and CO_2(g), in order to assess the resulting accuracy on the solubility calculation.

2. Mathematical formulation

In this section we present the mathematical formulation for thermodynamic equilibrium calculations of multiphase systems.

In what follows, we shall assume a chemical system composed of N species, where the i-th species is denoted by α_i and the vector of species by $\boldsymbol{\alpha} = [\alpha_1, \ldots, \alpha_N]^t$. In addition, we consider that there exist E elements from which these species can be formed, where the i-th element is denoted by ε_i and the vector of elements by $\boldsymbol{\varepsilon} = [\varepsilon_1, \ldots, \varepsilon_E]^t$. Finally, we assume that the chemical species are partitioned among Π phases, where α_i^π denotes the i-th species in the π-th phase, $\boldsymbol{\alpha}^\pi = [\alpha_1^\pi, \ldots, \alpha_{N_\pi}^\pi]^t$ denotes the vector of species in the π-th phase, and N_π denotes the number of species in the π-th phase.

2.1. Thermodynamic equilibrium

Assume a multiphase system whose chemical species participate in the following linearly independent equilibrium reactions:

$$0 \rightleftharpoons \sum_{i=1}^{N} \nu_{ji} \alpha_i \quad (j = 1, \ldots, M), \tag{1}$$

where ν_{ji} denotes the stoichiometric coefficient of the i-th species in the j-th reaction; and M the number of reactions, with $M < N$. The following sign convention is assumed for the stoichiometric coefficients ν_{ji}: negative for reactants, positive for products. We remark that the equilibrium reactions (1) can involve species from a single phase (i.e., homogeneous reactions) as well as species from different phases (i.e., heterogeneous reactions).

Since reactions (1) are considered to be in equilibrium, the composition of the chemical system must satisfy the following mass-action equations (see Appendix A):

$$\kappa_j = \prod_{i=1}^{N} a_i^{\nu_{ji}} \quad (j = 1, \ldots, M), \tag{2}$$

where $\kappa_j = \kappa_j(T, P)$ denotes the equilibrium constant of the j-th reaction; $a_i = a_i(T, P, \mathbf{n})$ the activity of the i-th chemical species; T and P the temperature and pressure of the system respectively; and $\mathbf{n} = [n_1, \ldots, n_N]^t$ the molar abundance vector of the system, with n_i denoting the number of moles of the i-th species.

The number of mass-action Eqs. (2) is not enough to resolve the equilibrium state of the system. Assuming that temperature and pressure are specified in the problem, it follows that there are N unknowns represented by the number of moles n_i of each species. Since there are only M mass-action equations, an additional of $E = N - M$ equilibrium constraints are required to resolve the problem.

Based on the previous discussion, we impose the following additional equilibrium constraints:

$$\sum_{i=1}^{N} g_{ji} n_i = h_j \quad (j = 1, \ldots, E), \tag{3}$$

where $g_{ji} = g_{ji}(T, P, \mathbf{n})$ and $h_j = h_j(T, P, \mathbf{n})$ are functions that will permit the imposition of a variety of equilibrium constraints as shown in the next section.

2.2. Equilibrium constraints

It is common to use mass-balance constraints in chemical equilibrium calculations. These are the natural equilibrium constraints, since they model the conservation of atoms of chemical elements. However, despite its frequent use, several other types of equilibrium constraints are particularly important and useful.

In geochemical modelling of natural waters, for example, one might be interested in imposing the pH of the solution, the total concentration of ionic species, and the electroneutrality condition of the mixture [10,13,31]. Below is a brief list of quantities that can be constrained at equilibrium:

- number of moles of a species;
- concentration of a species;
- activity or fugacity of a species;
- gas partial pressure;
- total volume of the multiphase system;
- the number of moles of an element.

Let us now describe how Eq. (3) can be configured to model some of the previously listed equilibrium constraints.

Imposition of number of moles of a species. The imposition of the number of moles of the k-th species at equilibrium is obtained by setting the j-th equilibrium constraint equation as:

$$g_{ji} = \delta_{ik} \quad \text{and} \quad h_j = n_k^\star, \tag{4}$$

where δ_{ik} is the Kronecker delta and $n_k^\star$ is the desired number of moles for the k-th species.

Imposition of charge balance. Macroscopically, an electrolyte solution is electrically neutral. Therefore, the following linear equation must be satisfied at equilibrium if the aqueous phase is to be charged balanced:

$$\sum_{i=1}^{N_{\pi_a}} z_i n_i^{\pi_a} = 0, \tag{5}$$

where π_a denotes the index of the aqueous phase; and z_i the electrical charge of the i-th aqueous species. Therefore, setting the j-th equilibrium constraint equation with the charge balance condition results in:

$$g_{ji} = z_i \delta_i^{\pi_a} \quad \text{and} \quad h_j = 0, \tag{6}$$

where $\delta_i^{\pi_a}$ is defined as:

$$\delta_i^{\pi_a} = \begin{cases} 1 & \text{if } \alpha_i \in \boldsymbol{\alpha}^{\pi_a} \\ 0 & \text{otherwise} \end{cases}. \tag{7}$$

Imposition of activity. Assuming that the activity of a species is known, this information can be used together with others to determine the compositional state of a chemical system. Frequently, the pH of a solution is readily available and so is the activity of species H^+, since $a_{H^+} = \exp_{10}(-\text{pH})$.

Since activity is a non-linear function, it is not possible to write it as a linear combination of variables n_i. Therefore, supposing that the j-th equilibrium constraint equation imposes the activity of the k-th species to $a_k^\star$, then the following is used:

$$g_{ji} = \delta_{ik} \quad \text{and} \quad h_j = \frac{n_k}{a_k} a_k^\star, \tag{8}$$

where a_k is the activity of the k-th species calculated with the composition state $\mathbf{n}^\ell$ at a iteration ℓ. The above approach has the effect of correcting $n_k^{\ell+1}$ based on the deviation of current a_k^ℓ from the specified $a_k^\star$.

Imposition of gas partial pressure. The partial pressure of the k-th species in the gaseous phase is given by:

$$P_k = y_k P, \tag{9}$$

where y_k is the molar fraction of k-th gaseous species given by:

$$y_k = \frac{n_k^g}{n_t^g}, \tag{10}$$

where g denotes the index of the gaseous species; and n_t^g the total number of moles in the gaseous phase. Combining the above two equations results in:

$$n_k^g = \frac{P_k}{P} n_t^g, \tag{11}$$

which is used to set the j-th equilibrium constraint with:

$$g_{ji} = \delta_{i,k_g} \quad \text{and} \quad h_j = \frac{P_k}{P} n_t^g. \tag{12}$$

Note that this constraint requires both pressure P and the composition of the gaseous species $\mathbf{n}^g$, which are available in the composition vector $\mathbf{n}$.

3. Numerical method

Section 2 described the mathematical formulation for the calculation of chemical equilibrium of multiphase systems subject to general equilibrium constraints. In this section we present the numerical methodology to compute the equilibrium state of the system, which requires the simultaneous solution of the non-linear mass-action Eqs. (2) and the equilibrium constraint Eqs. (3).

Initially we transform the mass-action Eqs. (2) by applying the natural logarithm to both sides and write the resulting equations in matrix form as:

$$\ln \boldsymbol{\kappa} = \boldsymbol{\nu} \ln \mathbf{a}, \tag{13}$$

where $\boldsymbol{\kappa} = [\kappa_1, \ldots, \kappa_M]^t$ is the vector of equilibrium constants; $\boldsymbol{\nu} = \{\nu_{ji}\}$ is the stoichiometric matrix of the equilibrium reactions (1); and $\mathbf{a} = [a_1, \ldots, a_N]^t$ is the vector of activities of the species. Similarly, we write the equilibrium constraint Eqs. (3) in matrix form as:

$$\mathbf{G}\mathbf{n} = \mathbf{h}. \tag{14}$$

In this work Eqs. (13) and (14) are solved with Newton's method, which is a well-known derivative-based root-finding algorithm that achieves second-order convergence near the solution. The algorithm consists of iteratively calculating new approximations of $\mathbf{n}$ through the matrix equation:

$$\mathbf{J}\delta\mathbf{n}^{l+1} = -\mathbf{f}, \tag{15}$$

where $\mathbf{f}$ denotes the residual function; $\mathbf{J}$ the Jacobian matrix; $\delta\mathbf{n}^{l+1}$ the composition step; and l the iteration number. Once $\delta\mathbf{n}^{l+1}$ is determined, then $\mathbf{n}^{l+1}$ can be calculated as:

$$\mathbf{n}^{l+1} = \mathbf{n}^{l} + \delta\mathbf{n}^{l+1}. \tag{16}$$

Note that the algorithm requires an initial guess $\mathbf{n}^0$, which should be near enough to the solution in order to prevent divergence.

3.1. Residual function and Jacobian matrix

From Eqs. (13) and (14), the residual function $\mathbf{f}$ is defined as:

$$\mathbf{f} = \begin{bmatrix} \mathbf{G}\mathbf{n} - \mathbf{h} \\ \boldsymbol{\nu} \ln \mathbf{a} - \ln \boldsymbol{\kappa} \end{bmatrix}. \tag{17}$$

One can now define the problem as:

$$\text{find } \mathbf{n} \text{ such that } \mathbf{f}(\mathbf{n}) = \mathbf{0},$$
$$\text{subject to } n_i > 0 \text{ for } i = 1, \ldots, N.$$

The later inequality constraint comes from the positivity of the composition variables. Note that we also restrict $\mathbf{n}$ to be component-wise non-zero, since every mass-action equation in (13) presumes the existence of every participating species in its corresponding equilibrium reaction in (1). Later we shall show how this restriction can be circumvented when a phase is not present in the equilibrium state.

Next, we derive the Jacobian matrix $\mathbf{J}$ from the residual vector $\mathbf{f}$, which is defined as $\mathbf{J} := \partial\mathbf{f}/\partial\mathbf{n}$. Therefore, from Eq. (17), it follows that:

$$\mathbf{J} = \begin{bmatrix} \mathbf{G} \\ \boldsymbol{\nu}\mathbf{A} \end{bmatrix}, \tag{18}$$

where $\mathbf{A}$ is the natural activity derivative matrix given by:

$$\mathbf{A} = \frac{\partial \ln \mathbf{a}}{\partial \mathbf{n}}. \tag{19}$$

As can be seen in Eq. (19), the calculation of the Jacobian matrix $\mathbf{J}$ requires the first order partial molar derivatives of the activity models $\mathbf{a} = \mathbf{a}(T, P, \mathbf{n})$.

3.2. Projection procedure

In order to ensure that $\mathbf{n}^{l+1}$ in Eq. (16) is component-wise positive, we project it to its feasible domain whenever one of its components become negative. This is done by slightly modifying Eq. (16) as:

$$n_i^{l+1} = n_i^{l} + y_i \delta n_i^{l+1}, \tag{20}$$

where y_i is a projection factor given by:

$$y_i = \begin{cases} \dfrac{(\omega - 1)n_i^l}{\delta n_i^{l+1}} & \text{if } n_i^l + \delta n_i^{l+1} \leqslant 0 \\ 1 & \text{otherwise} \end{cases}, \tag{21}$$

with $\omega \in (0, 1)$ being a projection constant.

The use of the projection factor in Eq. (21) guarantees that the positivity restriction on n_i^{l+1} is satisfied. This is done by replacing the i-th Newton step δn_i^{l+1} by $(\omega - 1)n_i^l$ whenever the former would lead the new iterate n_i^{l+1} to a negative state. Therefore, it is easy to see that the resulting equation becomes $n_i^{l+1} = \omega n_i^l$, where not only the length of the Newton step has changed, but also its direction.

Numerical experiments indicate that the choice of ω has a direct impact on the performance of the chemical equilibrium calculation. This is specially true when one phase in the system is missing in the final equilibrium state. Numerically, this is accompanied by the successive decrease of the total number of moles of the phase. A value of $\omega = 0.1$ accelerates this disappearance process; however, if a phase is not supposed to vanish from the calculation, the use of a relatively small projection value can compromise the convergence speed of the method. Therefore, in order to balance efficiency and correct behaviour of the calculation, we use a projection constant ω in the interval $[0.5, 0.7]$. Morel and Morgan [20] and Bethke [13] use a similar approach, where our projection constant ω would correspond to a fixed value of 0.5 in the published algorithms.

3.3. Stabilisation procedure

In Section 2, we formulated the chemical equilibrium problem for a multiphase system. However, depending on the conditions of temperature, pressure and equilibrium constraints, some phases might not be present at equilibrium. As a consequence, mass-action equations associated with non-existent phases will enforce unnecessary equilibrium conditions.

Determining the equilibrium phase assemblage of a multiphase system using the stoichiometric formulation is difficult and inelegant. However, unlike most geochemical solvers, we do not solve this issue with an ad hoc approach of addition and removal of phases to determine the correct phase assemblage. Instead, we apply a stabilisation procedure that aids the convergence of the stoichiometric method when potential phases in the calculation tend to disappearance. The heuristic technique we developed consists of a simple modification in the natural activity derivative matrix $\mathbf{A}$ (see Eq. 19).

The literature contains some efficient approaches for handling phase disappearance in flash equilibrium calculations. For instance, the negative flash technique developed by Whitson and Michelsen [32] is a well-regarded classic. Nevertheless, we find it difficult to adapt that technique to a stoichiometric methodology, since our approach does not use the Rachford–Rice equation commonly employed in flash calculations.

The difficult of handling phase disappearance, using the stoichiometric formulation, results from the premise that the solution is an interior point of the feasible domain. In other words, the molar composition of the species are positive. In Appendix A, when we write the first order optimality conditions for a minimum of the

Lagrange function (A.5), given by Eqs. (A.6) and (A.7), we are implicitly assuming that its minimum is achieved in an interior point. Therefore, whenever the equilibrium state is on the boundary of the feasible domain (i.e., some phases and their species have zero number of moles), the calculation will fail to converge.

The presentation of the stabilisation procedure requires the definition of an unstable phase. Let η_π denote the total number of moles in phase π, and η_t the total number of moles in the system. The π-th phase in the system is then said to be unstable, at iteration l, if the following conditions are satisfied:

$$\eta_\pi^l < \epsilon_s \eta_t^l \quad \text{and} \quad \eta_\pi^l < \eta_\pi^{l-1}, \tag{22}$$

where ϵ_s is a given stabilisation threshold value. In case $l = 0$, we use only the former condition. The threshold $\epsilon_s = 10^{-10}$ has proved to be satisfactory.

The stabilisation procedure consists of assuming that:

$$\frac{\partial \ln a_i}{\partial n_j} = \frac{\delta_{ij}}{n_i}, \tag{23}$$

for all species $\alpha_i \in \mathcal{U}$, where $\mathcal{U}$ denotes the set of all chemical species that belongs to an unstable phase. As a consequence, the matrix $\mathbf{A}$ in Eq. (19) needs to be modified as follows:

$$A_{ij} = \begin{cases} A_{ij} & \text{if } \alpha_i \notin \mathcal{U} \\ \dfrac{\delta_{ij}}{n_i} & \text{if } \alpha_i \in \mathcal{U} \end{cases}, \tag{24}$$

where A_{ij} denotes the entry (i,j) in matrix $\mathbf{A}$; and δ_{ij} is the Kronecker delta.

This approach has the following effects: (i) for a multi-species phase, it eliminates the dependency of the activity derivative of a species with respect to the others; and (ii) for a single-species phase, it assumes a large activity derivative for the species, that would be zero otherwise, resulting in a decrease of the equilibrium condition imposed by the mass-action equations associated with that species.

Finally, we remark that the Jacobian matrix $\mathbf{J}$ may become ill-conditioned before a phase is detected to be unstable. In our work, we assume that a matrix $\mathbf{M}$ in a linear system $\mathbf{Mx} = \mathbf{b}$ is ill-conditioned whenever the solution $\mathbf{x}$ does not satisfy $\|\mathbf{Mx} - \mathbf{b}\|/\|\mathbf{b}\| < \epsilon_{\text{ill}}$ for some small scalar ϵ_{ill}, where $\|\cdot\|$ denotes the ℓ^2-norm. In this case, we under-relax the Newton step $\delta\mathbf{n}^{l+1}$ by a factor $\theta \in (0,1)$. We have successfully circumvented ill-conditioned cases using $\theta = 0.1$ and $\epsilon_{\text{ill}} = 10^{-8}$.

3.4. Convergence criteria

The standard convergence criteria for Newton's method is adopted. Therefore, the iterative procedure should stop whenever the iterates satisfy:

$$\frac{\left\|\mathbf{n}^{l+1} - \mathbf{n}^{l}\right\|}{\|\mathbf{n}^{l+1}\| + 1} < \epsilon_n, \tag{25}$$

and the residual vector fulfils the condition:

$$\left\|\mathbf{f}^{l+1}\right\| < \epsilon_f, \tag{26}$$

where ϵ_n and ϵ_f are tolerance values.

However, the above criteria might never be fulfilled when unstable phases exist. This happens because the unstable reactions (i.e., reactions associated with unstable phases) do not achieve equilibrium in the sense of satisfying their respective mass-action equations. As such, the residual contribution from these equations does not necessarily become small enough to pass the convergence test given by condition (26). Hence, a modification of the previous convergence criteria is required whenever unstable phases exist.

Let $\hat{\mathbf{f}}$ denote the residual vector $\mathbf{f}$ with entries set to zero whenever they correspond to a mass-action equation of an unstable reaction. Then, the proposed modified convergence criteria requires that condition (26) be satisfied with $\hat{\mathbf{f}}$ instead, so that unstable reactions are neglected in the convergence check.

Note that heterogeneous reactions should be formulated as homogeneous reactions whenever possible in order to reduce the number of reactions excluded from the convergence check. Since the reactions can be linearly combined, this can be easily achieved if necessary.

4. Results and discussion

In this section we present results relevant to carbon dioxide storage in saline aquifers obtained using the chemical equilibrium method described in Section 3.

The following activity and fugacity coefficient models were used to perform the calculations:

- the HKF extended Debye–Hückel activity coefficient model for solvent water and ionic species [33–36];
- the Setschenow activity coefficient model for neutral aqueous species other than CO_2(aq);
- the activity coefficient models of Drummond [37] or Duan and Sun [38] for CO_2(aq);
- the fugacity coefficient models of Spycher and Reed [39], Spycher et al. [40] or Duan et al. [41] for CO_2(g) and H_2O(g).

The previous activity and fugacity coefficient models are presented in Appendix B for clarity and convenience. It is shown there how these coefficients can be used to compute the activities of the species so that the chemical equilibrium state of a system can be calculated.

Note that, with exception of the fugacity coefficient model of Spycher and Reed [39], the models of Spycher et al. [40] and Duan et al. [41] assume the gaseous phase as an ideal mixture. The implication of this is that the fugacity coefficient of each gas does not depend on phase composition, but only on temperature and pressure.

In our calculations the ideal fugacity coefficient model for H_2O(g) is used whenever the model of Duan et al. [41] is employed for CO_2(g). This follows from the lack of a non-iterative and efficient equation for the fugacity coefficient of H_2O(g) in the work of Duan et al. [41]. An alternative would be the use of the non-linear equations of state of Duan et al. [42], but these are prohibitively expensive to use in a reactive reservoir simulator. Note, however, that this assumption has little impact on the accuracy of our predictions of the solubility of CO_2.

The chemical potentials of the species were obtained using the equations of state of Helgeson and Kirkham [33], Helgeson et al. [43], Tanger and Helgeson [44], Shock and Helgeson [45] and Shock et al. [46]. The parameters of these equations were taken from the most recent database file of the software package SUPCRT92, from Johnson et al. [47]. Moreover, the density of water and its temperature and pressure derivatives, required for the calculation of the chemical potential of aqueous species, were calculated using the equation of state of Wagner and Pruss [48].

The chemical potentials of the species can be used to compute the equilibrium constants of reactions (1) using Eq. (A.13). This process can be skipped by using equilibrium constants available in databases such as those from geochemical packages EQ3/6 [9] or PHREEQC [10,11]. However, these databases have constants that are in general only temperature dependent, evaluated at a fixed pressure or at pressures corresponding to the vapour pressure of water. Therefore, at higher pressures, these data are no longer capable of yielding accurate equilibrium results.

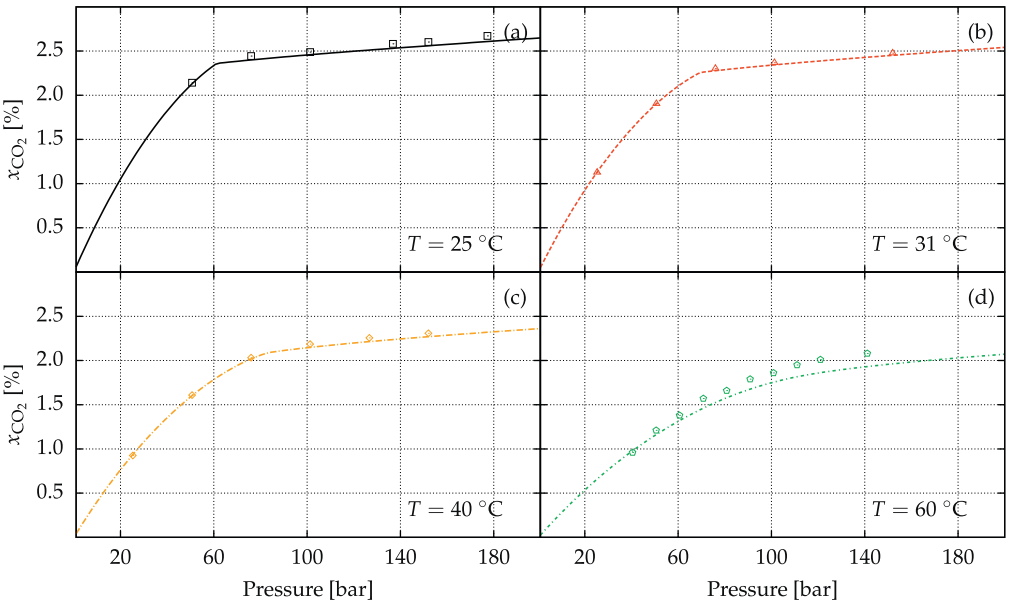

Fig. 1. Comparison of our calculations of CO_2 solubility in pure water (lines), using the activity coefficient model of Drummond [37] for CO_2(aq) and the fugacity coefficient model of Spycher et al. [40] for CO_2(g) and H_2O(g), with the experimental solubility data compiled in Spycher et al. [40] (points). The calculations assumed a CO_2–H_2O system composed of an aqueous and gaseous phase.

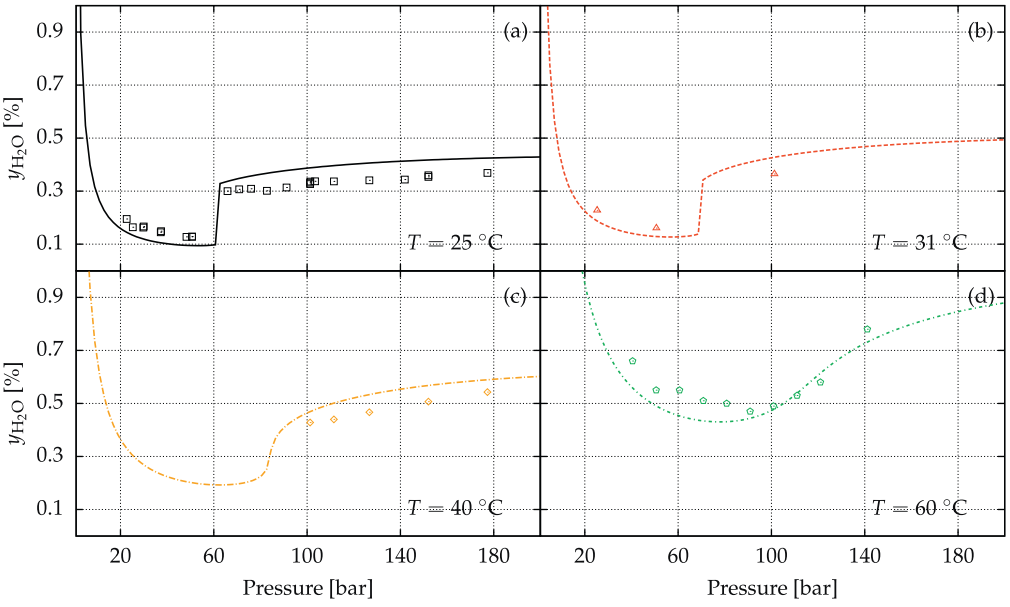

Fig. 2. Comparison of our calculations of H_2O solubility in the CO_2-rich phase (lines), using the activity coefficient model of Drummond [37] for CO_2(aq) and the fugacity coefficient model of Spycher et al. [40] for CO_2(g) and H_2O(g), with the experimental solubility data compiled in Spycher et al. [40] (points). The calculations assumed a CO_2–H_2O system composed of an aqueous and gaseous phase.

4.1. Mutual solubility of CO_2 and H_2O in brine

The capability to accurately model the solubility of CO_2 in brine is of utmost importance for understanding CO_2 storage in saline aquifers. This is because most of the injected CO_2 will eventually dissolve in the aqueous phase. Moreover, this dissolution will also acidify the aqueous phase, promoting geochemical reactions between fluid and rock. Therefore, correct predictions of these phenomena will depend on the accuracy of the calculated solubility of carbon dioxide in brines.

There are other aspects that should be considered when modelling the solubility of carbon dioxide in brines. One of them concerns the solubility of H_2O in the CO_2-rich phase. This is because near the injection well a considerable amount of water is evaporated to the injected supercritical CO_2. Since this evaporation is directly related to the precipitation of salts, which consequently decreases the local porosity and permeability of the rock, it can be argued that a certain degree of accuracy in the solubility calculation of vapour water in the CO_2-rich phase is required.

Other important aspects include the salt composition of the brine and its salinity. Frequently, brines contain significant concentrations of salts other than NaCl, such as $CaCl_2$, $MgCl_2$, KCl and so forth. As a consequence, a comprehensive accounting of these salts

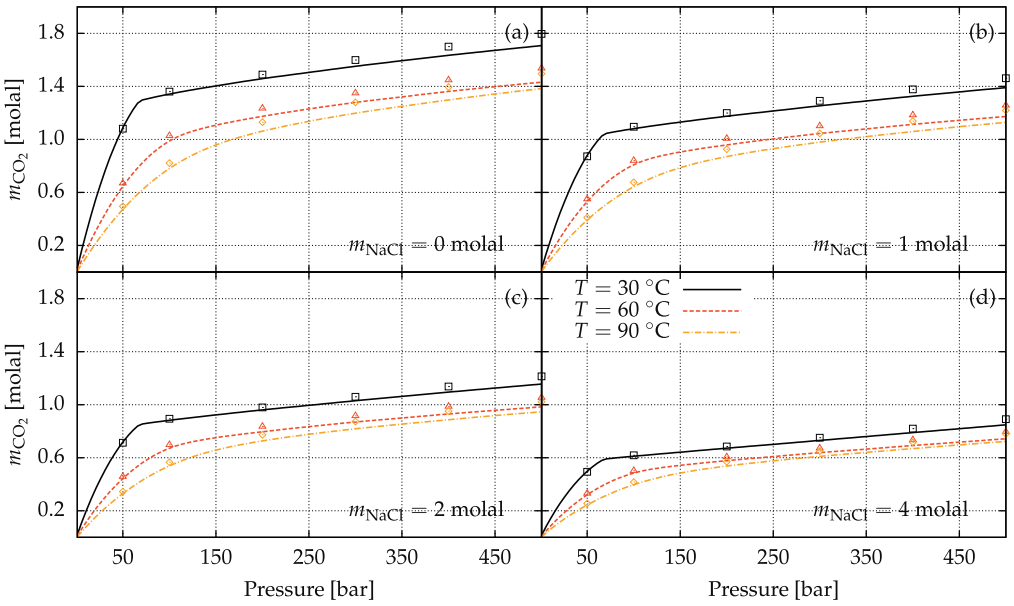

Fig. 3. Comparison of our calculations of CO_2 solubility in NaCl brine (lines), using the activity coefficient model of Drummond [37] for CO_2(aq) and the fugacity coefficient model of Spycher et al. [40] for CO_2(g) and H_2O(g), with the calculated solubility data of Duan and Sun [38] (points). The calculations assumed a CO_2–H_2O–NaCl system composed of an aqueous and gaseous phase.

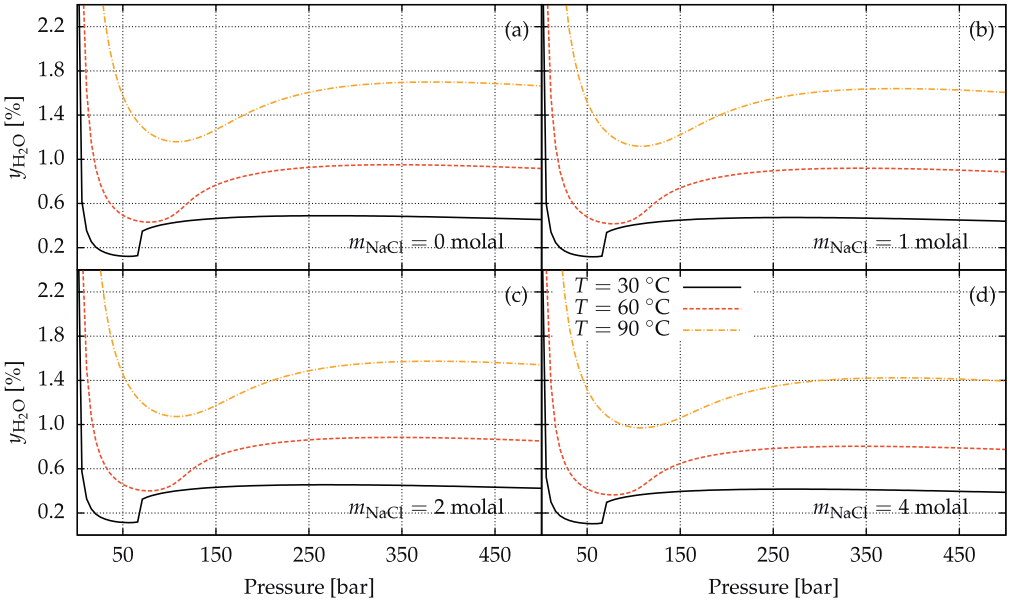

Fig. 4. Calculated H_2O solubility in the CO_2-rich phase, using the activity coefficient model of Drummond [37] for CO_2(aq) and the fugacity coefficient model of Spycher et al. [40] for CO_2(g) and H_2O(g). The calculations assumed a CO_2–H_2O–NaCl system composed of an aqueous and gaseous phase.

should not be neglected as this could lead to inaccurate results for the calculated CO_2 solubility.

We now present a series of figures and tables that show our calculations of mutual solubility of CO_2 and H_2O in brines. Most of these calculations were compared against experimental data in the literature or against solubility models.

Figs. 1 and 2 show the solubility of CO_2 in pure water and the solubility of H_2O in the CO_2-rich phase respectively, in terms of the molar fractions x_{CO_2} and y_{H_2O}. The experimental solubility data compiled in [40] were used to assess the accuracy of our calculations. The fugacity coefficient model of Spycher et al. [40] was used for the gaseous species CO_2(g) and H_2O(g). The chemical system was assumed to be composed of an aqueous and a gaseous phase. However, note that this gaseous phase predominantly containing CO_2 can in fact exist in the liquid or supercritical state depending on the temperature and pressure of the system.

Fig. 3 shows the solubility of CO_2 in NaCl brines of 0, 1, 2 and 4 molal, at temperatures 30, 60, 90 °C and pressures 1–500 bar. Fig. 4 shows the corresponding H_2O solubility in the CO_2-rich phase, where no comparisons with experimental data were made because of the lack of these at the assumed temperatures. These equilibrium calculations used the activity coefficient model of Drummond [37] for CO_2(aq) and the fugacity coefficient model of Spycher et al. [40] for CO_2(g) and H_2O(g). The calculations in Fig. 3 were compared against the calculated solubility from Duan and Sun [38] model, which was the same done as in [49].

Table 1
Comparison of our calculations of carbon dioxide solubility in pure water with the experimental solubility data of Tong et al. [29].

T (K)	P (bar)	x_{Exp} (%)	x_{SR} (%)	x_{SP} (%)	x_{DS} (%)	$Error_{SR}$ (%)	$Error_{SP}$ (%)	$Error_{DS}$ (%)
349.19	252.2	2.148	2.0160	2.0244	2.0436	6.143	5.755	4.860
349.13	183.1	2.017	1.9125	1.8684	1.8783	5.183	7.368	6.878
374.41	72.1	1.105	1.0059	1.0296	1.0349	8.973	6.824	6.344
374.18	144.4	1.711	1.5580	1.5868	1.6012	8.940	7.260	6.418
374.91	188.6	1.924	1.7508	1.7782	1.7927	9.001	7.580	6.826
374.15	223.4	2.048	1.8449	1.8862	1.9126	9.919	7.900	6.613
374.99	272.6	2.189	1.9067	2.0123	2.0529	12.895	8.073	6.220
					Average	**8.722**	**7.251**	**6.308**

Note: In this and subsequent tables, x_{Exp} denotes experimental molar fraction of aqueous CO_2. x_{SR}, x_{SP} and x_{DS} denote the calculated molar fraction of aqueous CO_2 using respectively the fugacity coefficient models of Spycher and Reed [39], Spycher et al. [40] and Duan et al. [41] for the gaseous mixture H_2O–CO_2. $Error_{SR}$, $Error_{SP}$ and $Error_{DS}$ denote respectively the percentage deviation of x_{SR}, x_{SP} and x_{DS} from x_{Exp}.

Table 2
Comparison of our calculations of carbon dioxide solubility in NaCl brine, using the activity coefficient model of Duan and Sun [38] for CO_2(aq), with the experimental solubility data of Hou et al. [30].

T (K)	P (bar)	m_{NaCl}	x_{Exp} (%)	x_{SR} (%)	x_{SP} (%)	x_{DS} (%)	$Error_{SR}$ (%)	$Error_{SP}$ (%)	$Error_{DS}$ (%)
323.15	27.82	2.5	0.492	0.5046	0.5164	0.5141	2.567	4.951	4.488
	57.39		0.875	0.8666	0.8928	0.8848	0.965	2.034	1.117
	87.3		1.146	1.1115	1.1232	1.1160	3.008	1.986	2.618
	117.73		1.238	1.2761	1.2136	1.2090	3.077	1.970	2.345
	150.2		1.293	1.3866	1.2654	1.2530	7.242	2.136	3.093
	182.11		1.335	1.4460	1.3064	1.2920	8.312	2.145	3.220
						Average	**4.195**	**2.537**	**2.813**
373.15	26.13	2.5	0.254	0.2827	0.2862	0.2874	11.304	12.676	13.135
	57.42		0.532	0.5491	0.5610	0.5631	3.213	5.451	5.845
	87.89		0.739	0.7458	0.7641	0.7675	0.914	3.391	3.861
	118.67		0.899	0.8969	0.9167	0.9224	0.228	1.969	2.606
	149.21		1.032	1.0100	1.0268	1.0344	2.129	0.503	0.234
	180.13		1.139	1.0957	1.1099	1.1148	3.800	2.559	2.121
						Average	**3.598**	**4.425**	**4.634**
423.15	26.43	2.5	0.193	0.2360	0.2379	0.2401	22.272	23.259	24.430
	57.66		0.440	0.4560	0.4638	0.4744	3.626	5.404	7.810
	86.00		0.640	0.6364	0.6504	0.6672	0.569	1.622	4.249
	116.04		0.824	0.7939	0.8152	0.8397	3.653	1.068	1.901
	148.81		1.014	0.9331	0.9634	0.9972	7.980	4.994	1.652
	177.94		1.137	1.0321	1.0722	1.1149	9.230	5.700	1.944
						Average	**7.888**	**7.008**	**6.998**
323.15	29.83	4.0	0.403	0.4196	0.4298	0.4277	4.112	6.652	6.133
	59.54		0.689	0.6945	0.7153	0.7087	0.798	3.820	2.854
	89.53		0.871	0.8807	0.8873	0.8823	1.111	1.866	1.292
	120.17		0.956	1.0073	0.9537	0.9489	5.365	0.237	0.743
	149.59		0.997	1.0866	0.9919	0.9817	8.988	0.513	1.533
	179.54		1.025	1.1347	1.0246	1.0128	10.700	0.037	1.193
						Average	**5.179**	**2.188**	**2.291**
373.15	29.51	4.0	0.251	0.2562	0.2597	0.2606	2.076	3.471	3.836
	60.68		0.446	0.4618	0.4721	0.4737	3.553	5.860	6.204
	89.16		0.620	0.6058	0.6206	0.6231	2.288	0.103	0.503
	120.03		0.752	0.7263	0.7420	0.7461	3.420	1.331	0.780
	149.24		0.857	0.8135	0.8267	0.8321	5.079	3.535	2.910
	181.62		0.934	0.8869	0.8977	0.9009	5.048	3.889	3.544
						Average	**3.577**	**3.031**	**2.963**
423.15	30.93	4.0	0.195	0.2219	0.2239	0.2262	13.786	14.830	16.020
	58.16		0.375	0.3732	0.3795	0.3875	0.482	1.190	3.346
	88.57		0.556	0.5261	0.5377	0.5508	5.376	3.299	0.928
	119.22		0.709	0.6524	0.6697	0.6890	7.990	5.536	2.827
	149.79		0.844	0.7554	0.7793	0.8053	10.503	7.664	4.586
	180.79		0.972	0.8397	0.8720	0.9051	13.611	10.293	6.879
						Average	**8.625**	**7.135**	**5.764**

Note: m_{NaCl} denotes the salinity of the NaCl brine in molality scale.

Tables 1–6 present the solubility results for carbon dioxide in brines of different salt composition and salinity, at temperature and pressure conditions representative of saline aquifers. The experimental solubility data used to assess the accuracy of our calculations were taken from the recent measurements of Tong et al. [29] and Hou et al. [30].

Table 3
Comparison of our calculations of carbon dioxide solubility in NaCl brine, using the activity coefficient model of Drummond [37] for CO_2(aq), with the experimental solubility data of Hou et al. [30].

T (K)	P (bar)	m_{NaCl}	x_{Exp} (%)	x_{SR} (%)	x_{SP} (%)	x_{DS} (%)	$Error_{SR}$ (%)	$Error_{SP}$ (%)	$Error_{DS}$ (%)
323.15	27.82	2.5	0.492	0.4938	0.5053	0.5030	0.362	2.695	2.242
	57.39		0.875	0.8580	0.8840	0.8761	1.941	1.029	0.120
	87.30		1.146	1.1059	1.1176	1.1104	3.496	2.479	3.108
	117.73		1.238	1.2723	1.2100	1.2054	2.770	2.261	2.635
	150.20		1.293	1.3832	1.2623	1.2499	6.976	2.378	3.332
	182.11		1.335	1.4416	1.3024	1.2881	7.983	2.441	3.514
						Average	**3.921**	**2.214**	**2.492**
373.15	26.13	2.5	0.254	0.2777	0.2811	0.2822	9.318	10.665	11.115
	57.42		0.532	0.5492	0.5611	0.5632	3.232	5.470	5.864
	87.89		0.739	0.7524	0.7709	0.7744	1.819	4.318	4.792
	118.67		0.899	0.9099	0.9300	0.9358	1.214	3.443	4.089
	149.21		1.032	1.0283	1.0454	1.0531	0.358	1.297	2.048
	180.13		1.139	1.1183	1.1328	1.1378	1.815	0.548	0.102
						Average	**2.959**	**4.290**	**4.668**
423.15	26.43	2.5	0.193	0.2296	0.2314	0.2336	18.956	19.916	21.055
	57.66		0.440	0.4541	0.4619	0.4724	3.198	4.968	7.364
	86.00		0.640	0.6414	0.6555	0.6724	0.213	2.422	5.069
	116.04		0.824	0.8074	0.8290	0.8539	2.019	0.610	3.629
	148.81		1.014	0.9560	0.9870	1.0218	5.717	2.658	0.765
	177.94		1.137	1.0632	1.1045	1.1485	6.495	2.860	1.007
						Average	**6.100**	**5.572**	**6.482**
323.15	29.83	4.0	0.403	0.4010	0.4108	0.4088	0.505	1.924	1.427
	59.54		0.689	0.6743	0.6946	0.6881	2.128	0.807	0.131
	89.53		0.871	0.8598	0.8663	0.8614	1.282	0.544	1.104
	120.17		0.956	0.9846	0.9323	0.9275	2.995	2.482	2.976
	149.59		0.997	1.0609	0.9684	0.9585	6.413	2.864	3.861
	179.54		1.025	1.1050	0.9978	0.9862	7.801	2.657	3.783
						Average	**3.521**	**1.880**	**2.214**
373.15	29.51	4.0	0.251	0.2521	0.2556	0.2565	0.449	1.822	2.181
	60.68		0.446	0.4653	0.4757	0.4773	4.338	6.661	7.008
	89.16		0.620	0.6166	0.6317	0.6342	0.553	1.880	2.287
	120.03		0.752	0.7435	0.7596	0.7638	1.128	1.011	1.574
	149.24		0.857	0.8352	0.8488	0.8543	2.545	0.961	0.318
	181.62		0.934	0.9117	0.9229	0.9262	2.384	1.193	0.838
						Average	**1.900**	**2.254**	**2.368**
423.15	30.93	4.0	0.195	0.2201	0.2221	0.2244	12.870	13.906	15.087
	58.16		0.375	0.3803	0.3867	0.3949	1.411	3.116	5.313
	88.57		0.556	0.5450	0.5570	0.5706	1.973	0.178	2.634
	119.22		0.709	0.6830	0.7012	0.7213	3.669	1.101	1.734
	149.79		0.844	0.7966	0.8219	0.8492	5.615	2.623	0.622
	180.79		0.972	0.8903	0.9245	0.9596	8.407	4.890	1.273
						Average	**5.658**	**4.302**	**4.444**

Note: m_{NaCl} denotes the salinity of the NaCl brine in molality scale.

Table 1 presents the results of our solubility calculations in pure water, from which we can assess the accuracy of the estimates. The equilibrium calculations were performed using different fugacity coefficient models for the gaseous mixture CO_2–H_2O. The results indicate that the fugacity coefficient model of Duan et al. [41] yields the most accurate results, where an average percentage deviation of 6.3% from the experimental data can be observed.

Tables 2 and 3 show the calculated solubility of CO_2 in NaCl brines at high salinities using, respectively, the activity coefficient models of Duan and Sun [38] and Drummond [37] for the aqueous species CO_2(aq). Between these two activity coefficient models, it can be affirmed that the latter is slightly more accurate for NaCl brines. As to the fugacity coefficient models for CO_2(g), we observe again that the model of Duan et al. [41] yields the most accurate results, where the percentage deviations are in general less than 7%. This good agreement of the results demonstrate that this model is accurate enough for engineering applications.

In order to have a qualitative perception of the accuracy of the fugacity coefficient models of Spycher and Reed [39], Spycher et al. [40] and Duan et al. [41], we refer the reader to Figs. 5,6. The qualitative comparison of the activity coefficient models of Duan and Sun [38] and Drummond [37] can be made in Figs. 7 and 8. Observing these figures one realises that the fugacity coefficient of Duan et al. [41] for CO_2(g) results in more accurate solubility calculations. Moreover, the activity coefficient model of Drummond [37] for CO_2(aq) performs better than the one of Duan and Sun [38], except at low temperatures, and high pressures and salinities, as seen in Fig. 8(a).

Tables 4–6 indicate that the activity coefficient model of Drummond [37] for CO_2(aq) is not suitable for brines with salt compositions other than pure NaCl. The solubility calculations in NaCl + KCl brine, with KCl salt in low proportion, show that the Duan and Sun [38] model is slightly superior in such cases. In addition, for the solubility calculations in $MgCl_2$ and $CaCl_2$ brines, it becomes evident that the Duan and Sun [38] model is considerably superior than the Drummond [37] model for non-NaCl brines.

Table 4
Comparison of our calculations of carbon dioxide solubility in NaCl–KCl brine, using the fugacity coefficient model of Duan et al. [41] for CO_2(g), with the experimental solubility data of Tong et al. [29].

T (K)	P (bar)	x_{Exp} (%)	$x_{DuanSun}$ (%)	$x_{Drummond}$ (%)	$Error_{DuanSun}$ (%)	$Error_{Drummond}$ (%)
309.14	11.9	0.384	0.4212	0.4129	9.700	7.532
308.90	37.4	1.180	1.1193	1.1070	5.148	6.187
324.11	10.7	0.322	0.2789	0.2724	13.384	15.419
324.10	43.5	1.062	0.9387	0.9275	11.615	12.663
343.83	17.7	0.295	0.3373	0.3293	14.334	11.624
343.92	36.1	0.642	0.6314	0.6205	1.656	3.349
343.88	136.9	1.580	1.4427	1.4324	8.688	9.342
345.04	102.5	1.381	1.2803	1.2687	7.290	8.135
374.92	29.9	0.409	0.4063	0.3950	0.668	3.421
374.92	69.6	0.872	0.8259	0.8103	5.290	7.078
374.89	147.8	1.415	1.3196	1.3046	6.744	7.802
424.67	40.0	0.407	0.4382	0.4197	7.658	3.113
424.62	86.8	0.869	0.8625	0.8356	0.752	3.849
424.64	171.6	1.460	1.4174	1.3890	2.920	4.863
				Average	**6.846**	**7.455**

Note: The salinity of the NaCl + KCl brine is $m_{NaCl} = 0.910$ molal and $m_{KCl} = 0.143$ molal. $x_{DuanSun}$ and $x_{Drummond}$ denote the calculated aqueous molar fraction of CO_2 using respectively the activity coefficient models of Duan and Sun [38] and Drummond [37] for CO_2(aq). $Error_{DuanSun}$ and $Error_{Drummond}$ denote respectively the percentage deviation of $x_{DuanSun}$ and $x_{Drummond}$ from x_{Exp}.

Table 5
Comparison of our calculations of carbon dioxide solubility in $MgCl_2$ brine, using the fugacity coefficient model of Duan et al. [41] for CO_2(g), with the experimental solubility data of Tong et al. [29].

T (K)	P (bar)	m_{MgCl_2}	x_{Exp} (%)	$x_{DuanSun}$ (%)	$x_{Drummond}$ (%)	$Error_{DuanSun}$ (%)	$Error_{Drummond}$ (%)
309.58	12.5	1.0	0.382	0.3629	0.2850	5.007	25.387
309.83	42.4	1.0	1.085	0.9930	0.7949	8.482	26.740
324.41	16.5	1.0	0.366	0.3470	0.2805	5.193	23.351
324.37	56.8	1.0	1.041	0.9365	0.7719	10.036	25.850
343.90	20.4	1.0	0.344	0.3234	0.2668	6.002	22.430
344.20	76.2	1.0	0.996	0.9118	0.7696	8.456	22.727
344.93	305.8	1.0	1.532	1.4529	1.2439	5.162	18.806
374.24	26.4	1.0	0.294	0.3076	0.2578	4.612	12.308
374.22	102.5	1.0	1.005	0.9023	0.7776	10.219	22.630
374.91	349.3	1.0	1.609	1.4844	1.3090	7.744	18.644
424.03	39.5	1.0	0.345	0.3632	0.3122	5.265	9.495
423.95	126.3	1.0	0.980	0.9498	0.8448	3.083	13.800
424.63	197.4	1.0	1.310	1.2619	1.1400	3.673	12.977
424.63	283.7	1.0	1.609	1.5032	1.3778	6.578	14.367
344.68	130.9	5.0	0.370	0.3372	0.3512	8.871	5.092
344.98	312.0	5.0	0.471	0.4477	0.4406	4.941	6.457
374.72	75.5	5.0	0.257	0.2259	0.2556	12.112	0.558
374.68	156.0	5.0	0.384	0.3425	0.3962	10.804	3.174
375.02	205.8	5.0	0.414	0.3851	0.4441	6.972	7.276
424.39	47.0	5.0	0.131	0.1327	0.1607	1.301	22.678
424.33	103.4	5.0	0.231	0.2465	0.3191	6.721	38.138
424.49	161.8	5.0	0.355	0.3330	0.4421	6.194	24.539
					Average	**6.701**	**17.156**

Note: m_{MgCl_2} denotes the salinity of the $MgCl_2$ brine in molality scale.

In [49], the solubility of H_2O in the CO_2-rich phase was calculated for CO_2-brine system. However, at that time no experimental data were available for assessing the accuracy of their calculations. In Figs. 9 and 10 we show a comparison of our calculations of H_2O solubility in the CO_2-rich phase with the experimental solubility data of Hou et al. [30]. These were performed assuming an aqueous phase containing 2.5 and 4.0 molal of NaCl and a gaseous phase. Different fugacity coefficient models were used for the gaseous species CO_2(g) and H_2O(g). From these figures, it can be observed that the fugacity coefficient model of Duan et al. [41] achieves better accuracy than the other models, except at higher temperatures, where the model of Spycher et al. [40] presents a closer agreement with the experimental data. However, we remark that this model was developed for temperatures 12–100 °C, as stated in [40].

4.2. Phase behaviour of CO_2–H_2O–rock systems

Fig. 11 shows the ability of the chemical equilibrium method to determine the stable phase assemblage of CO_2–H_2O–mineral systems, where the minerals assumed were halite, calcite, and magnesite respectively. The calculations were made by assuming a fixed feed molar fraction z_{Min} of each mineral component. The feed molar fraction z_{CO_2} of component CO_2 was varied from 0 to $1 - z_{min}$ and the feed molar fraction z_{H_2O} of component H_2O was computed by:

$$z_{H_2O} = 1 - z_{CO_2} - z_{Min}. \quad (27)$$

From the molar fractions of the components, the molar abundance of each element was determined, which served as input to the equilibrium calculation.

Table 6
Comparison of our calculations of carbon dioxide solubility in $CaCl_2$ brine, using the fugacity coefficient model of Duan et al. [41] for CO_2(g), with the experimental solubility data of Tong et al. [29].

T (K)	P (bar)	m_{CaCl_2}	x_{Exp} (%)	$x_{DuanSun}$ (%)	$x_{Drummond}$ (%)	$Error_{DuanSun}$ (%)	$Error_{Drummond}$ (%)
309.67	15.3	1.0	0.448	0.4343	0.3490	3.058	22.091
309.28	40.1	1.0	1.036	0.9639	0.7854	6.962	24.191
344.67	25.8	1.0	0.402	0.3940	0.3319	1.983	17.449
344.35	73.0	1.0	0.976	0.8864	0.7596	9.185	22.177
344.95	310.2	1.0	1.510	1.4567	1.2668	3.527	16.104
374.70	31.3	1.0	0.377	0.3580	0.3068	5.034	18.619
374.70	100.2	1.0	0.934	0.8887	0.7798	4.853	16.510
374.88	373.8	1.0	1.613	1.5136	1.3603	6.163	15.669
424.13	43.9	1.0	0.392	0.3968	0.3441	1.213	12.225
424.10	127.7	1.0	1.001	0.9573	0.8567	4.362	14.417
424.43	268.2	1.0	1.581	1.4639	1.3462	7.409	14.854
424.40	82.9	3.0	0.380	0.3508	0.2967	7.687	21.931
424.39	271.1	3.0	0.807	0.7236	0.6605	10.332	18.149
424.38	379.9	3.0	0.903	0.8315	0.7737	7.919	14.318
344.72	61.2	5.0	0.272	0.2257	0.2308	17.023	15.131
344.70	145.4	5.0	0.357	0.3480	0.3621	2.519	1.428
344.96	345.2	5.0	0.511	0.4615	0.4467	9.692	12.583
374.72	76.1	5.0	0.266	0.2251	0.2550	15.373	4.118
374.72	169.1	5.0	0.402	0.3508	0.4061	12.741	1.008
374.72	342.5	5.0	0.484	0.4724	0.5242	2.403	8.313
424.43	46.4	5.0	0.141	0.1311	0.1586	7.019	12.505
424.42	105.3	5.0	0.239	0.2493	0.3233	4.323	35.271
					Average	**6.854**	**15.412**

Note: m_{CaCl_2} denotes the salinity of the $CaCl_2$ brine in molality scale.

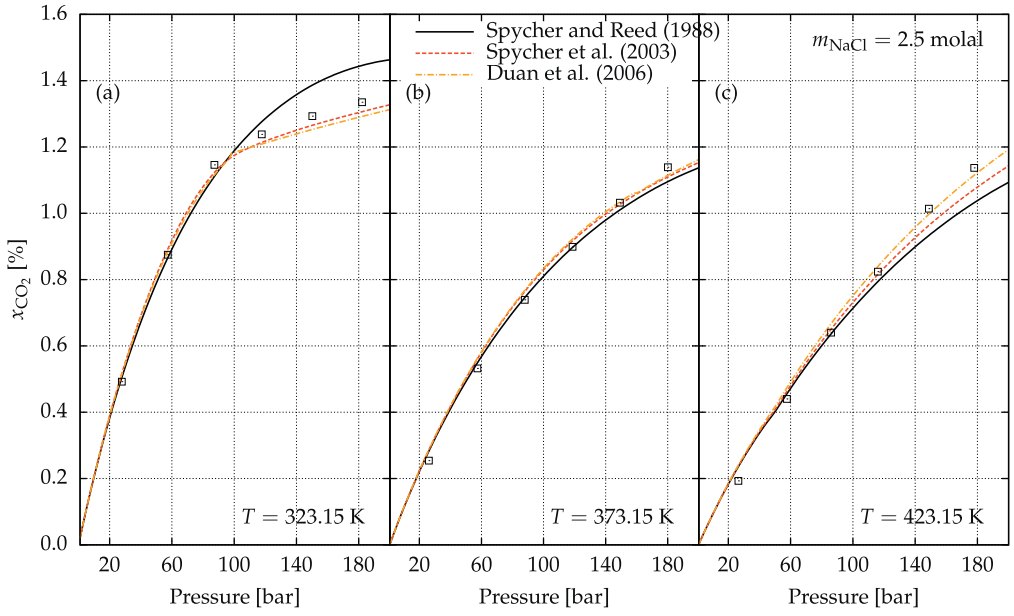

Fig. 5. Comparison of our calculations of CO_2 solubility in 2.5 molal NaCl brine (lines), using the activity coefficient model of Duan and Sun [38] for CO_2(aq) and the fugacity coefficient models of Spycher and Reed [39], Spycher et al. [40] and Duan et al. [41] for CO_2(g) and H_2O(g), with the experimental solubility results of Hou et al. [30] (points). The calculations assumed a CO_2-H_2O-NaCl system composed of an aqueous and gaseous phase.

From Fig. 11, some discontinuities in the concentration of the aqueous species can be seen. These discontinuities characterise a change in the phase assemblage of the system. When z_{CO_2} assumes small values, only the aqueous phase exists in the system, which is represented by the steep concentration line of CO_2(aq). Then, a gaseous phase is formed for intermediate values of z_{CO_2}, while all the mineral is still dissolved in the aqueous phase. As z_{CO_2} further increases, a solid phase appears in the system, represented by the planar region in the graph. Finally, for values of z_{CO_2} near to its limit, we have the aqueous phase being fully evaporated to the gaseous phase, resulting in zero concentrations for the aqueous species.

The previous equilibrium calculations only considered a single mineral. We now present an equilibrium calculation for the more complex system CO_2–H_2O–halite–calcite–magnesite, which is composed of an aqueous and gaseous phase plus three mineral solid phases. The calculations were performed at a high temperature and pressure condition, $T = 100\ ^\circ C$ and $P = 300$ bar, using the elemental molar abundance given in Table 7. The fugacity coefficient model of Duan et al. [41] was used for CO_2(g) and the activity

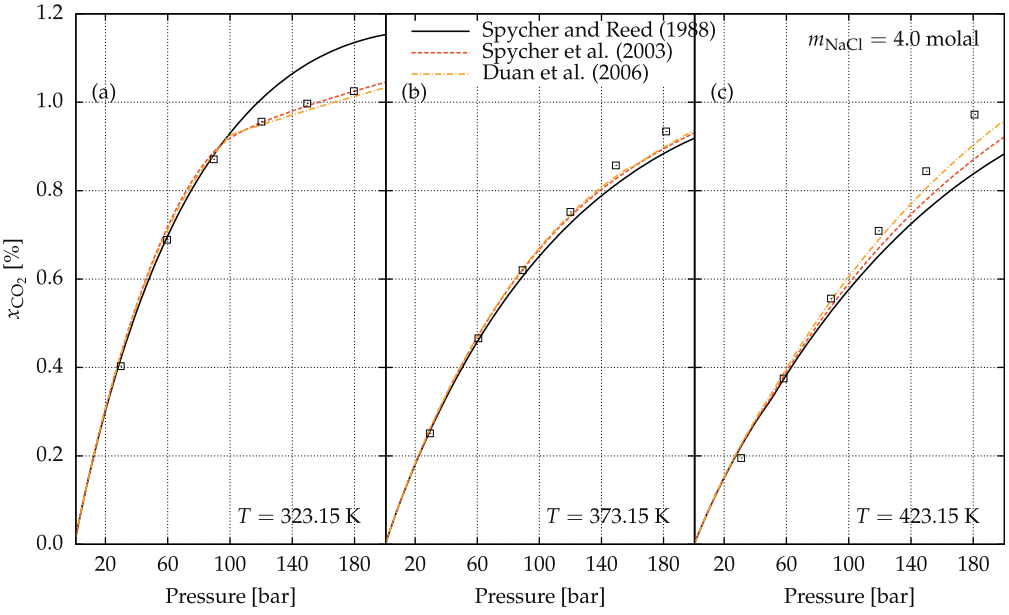

Fig. 6. Comparison of our calculations of CO_2 solubility in 4.0 molal NaCl brine (lines), using the activity coefficient model of Duan and Sun [38] for CO_2(aq) and the fugacity coefficient models of Spycher and Reed [39], Spycher et al. [40] and Duan et al. [41] for CO_2(g) and H_2O(g), with the experimental solubility results of Hou et al. [30] (points). The calculations assumed a CO_2–H_2O–NaCl system composed of an aqueous and gaseous phase.

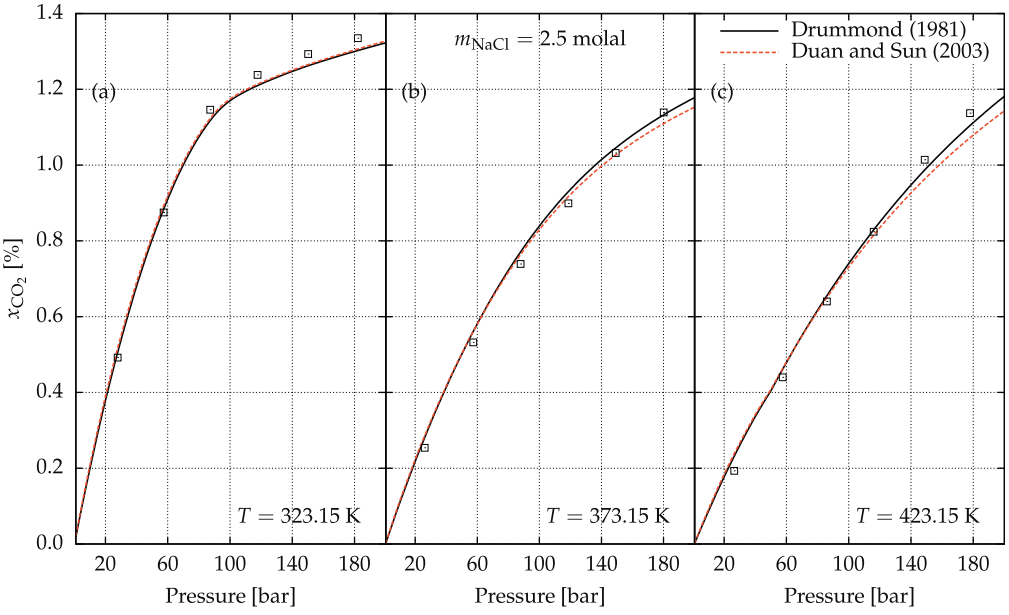

Fig. 7. Comparison of our calculations of CO_2 solubility in 2.5 molal NaCl brine (lines), using the activity coefficient models of Duan and Sun [38] and Drummond [37] for CO_2(aq) and the fugacity coefficient model of Spycher et al. [40] for CO_2(g) and H_2O(g), with the experimental solubility results of Hou et al. [30] (points). The calculations assumed a CO_2–H_2O–NaCl system composed of an aqueous and gaseous phase.

coefficient model of Duan and Sun [38] was used for CO_2(aq). The result of the calculation is shown in Table 8, where it can be noticed that the mineral halite is fully dissolved into the aqueous phase.

Using the solubility model developed by Duan et al. [41] for CO_2 in brine, we can compare our predictions with theirs. First, we calculate from Table 8 the following stoichiometric ionic molalities:

$$m_{Na^+} = 3.978, \quad m_{Ca^{2+}} = 2.283 \cdot 10^{-2},$$
$$m_{Cl^-} = 3.978, \quad m_{Mg^{2+}} = 1.503 \cdot 10^{-2},$$

in units of molal. Then, using the same temperature and pressure, and the previous molalities as input to their solubility model, we obtain $m^{Duan}_{CO_2} = 0.648$ molal.

In order to calculate m_{CO_2} from Table 8, however, we remark that there are several species in the aqueous phase containing carbon. Therefore, accounting for all these species, we determine $m_{CO_2} = 0.676$ molal. This result has approximately 4.3% of relative deviation from the one obtained using the solubility model of Duan et al. [41].

4.3. Accuracy of existing geochemical solvers

In this section we assess the accuracy of two solvers commonly used for the calculation of CO_2 solubility in NaCl brines. Our objective is to verify how well they reproduce the recent solubility experiments of Hou et al. [30] at high temperatures, pressures

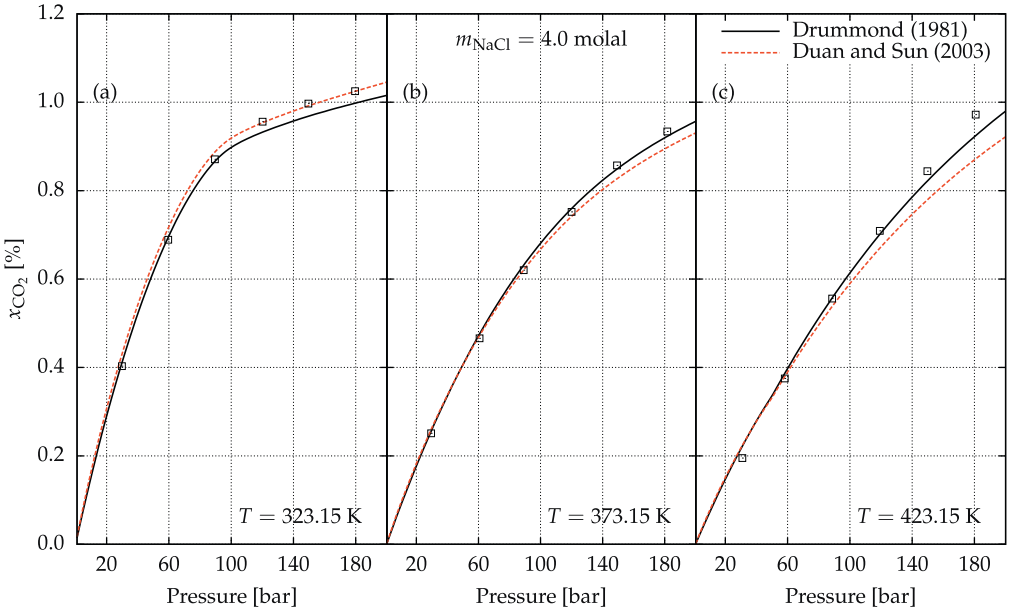

Fig. 8. Comparison of our calculations of CO_2 solubility in 4.0 molal NaCl brine (lines), using the activity coefficient models of Duan and Sun [38] and Drummond [37] for CO_2(aq) and the fugacity coefficient model of Spycher et al. [40] for CO_2(g) and H_2O(g), with the experimental solubility results of Hou et al. [30] (points). The calculations assumed a CO_2–H_2O–NaCl system composed of an aqueous and gaseous phase.

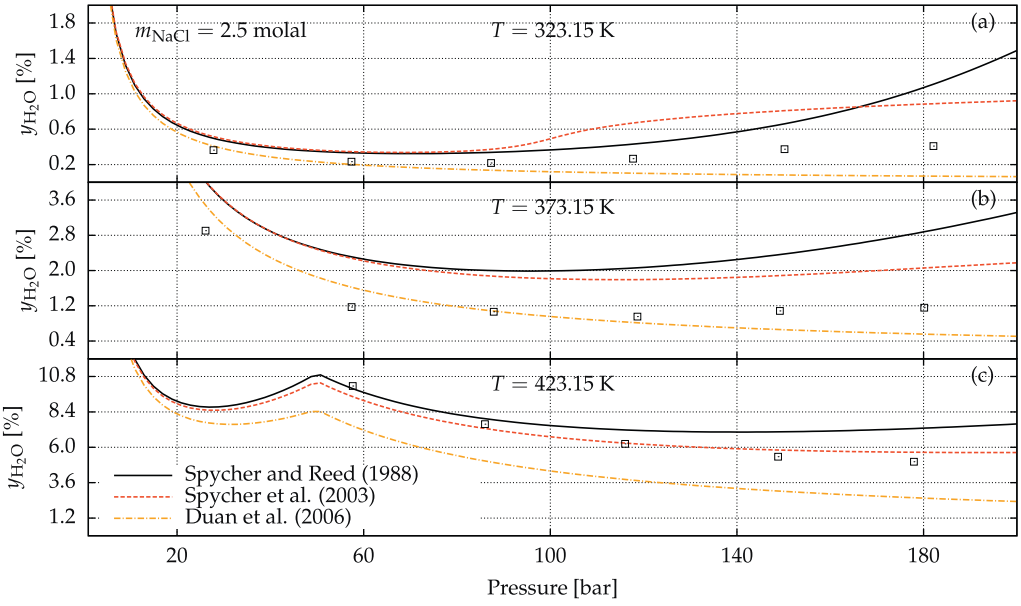

Fig. 9. Comparison of our calculations of H_2O solubility in the CO_2-rich phase (lines), using the activity coefficient model of Duan and Sun [38] for CO_2(aq) and the fugacity coefficient models of Spycher and Reed [39], Spycher et al. [40] and Duan et al. [41] for CO_2(g) and H_2O(g), with the experimental solubility results of Hou et al. [30] (points). The calculations assumed a CO_2–H_2O–NaCl system composed of an aqueous and gaseous phase, where the aqueous phase contains 2.5 molal of NaCl.

and salinities. Moreover, this analysis serves to determine under which conditions such solvers are not reliable.

The geochemical package PHREEQC v3.0 [11] and the well-known solubility model of Duan and Sun [38] are used for the solubility calculations. In a recent update of PHREEQC, several new modelling features were implemented, where Pitzer aqueous models are used for high-salinity brines and the Peng–Robinson equation of state is used to calculate the fugacity coefficients of gases at high pressures, allowing for a more accurate gas solubility calculation. The thermodynamic model developed by Duan and Sun [38], based on the specific interaction model of Pitzer with a parameterisation of a large amount of experimental data in the literature, allows the calculation of CO_2 solubility in NaCl brines for temperatures 273–533 K, pressures 0–2000 bar and salinities 0–4.3 molal.

Table 9 presents a comparison of the solubility results using the previous solvers with the experimental data of Hou et al. [30]. Note that we have also compared these calculations with the ones obtained using our numerical method presented in Section 3. We used the activity coefficient model of Drummond [37] for CO_2(aq) and the fugacity coefficient model of Spycher et al. [40] for CO_2(g) and H_2O(g).

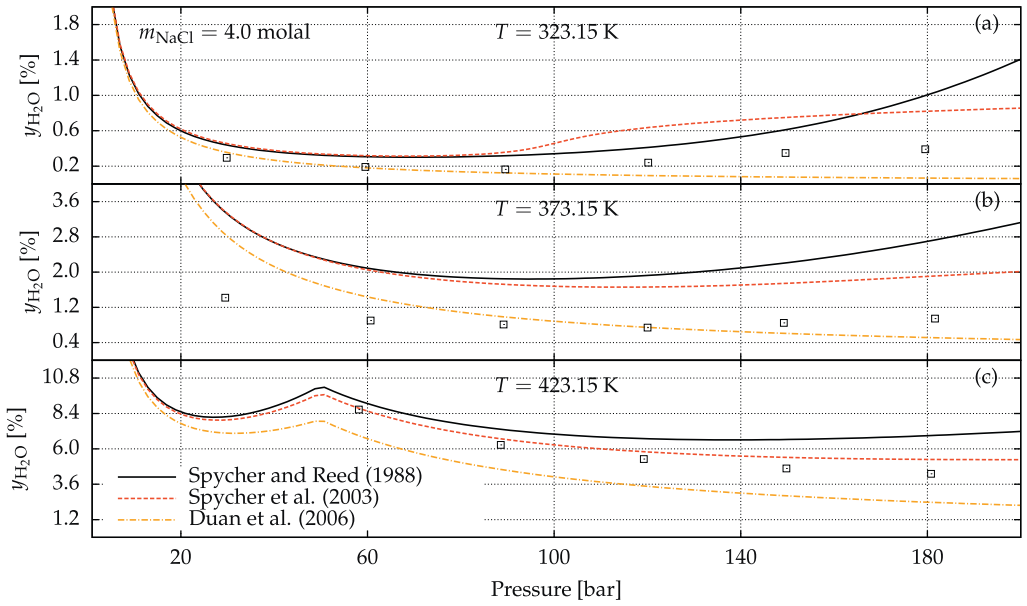

Fig. 10. Comparison of our calculations of H_2O solubility in the CO_2-rich phase (lines), using the activity coefficient model of Duan and Sun [38] for CO_2(aq) and the fugacity coefficient models of Spycher and Reed [39], Spycher et al. [40] and Duan et al. [41] for CO_2(g) and H_2O(g), with the experimental solubility results of Hou et al. [30] (points). The calculations assumed a CO_2–H_2O–NaCl system composed of an aqueous and gaseous phase, where the aqueous phase contains 4.0 molal of NaCl.

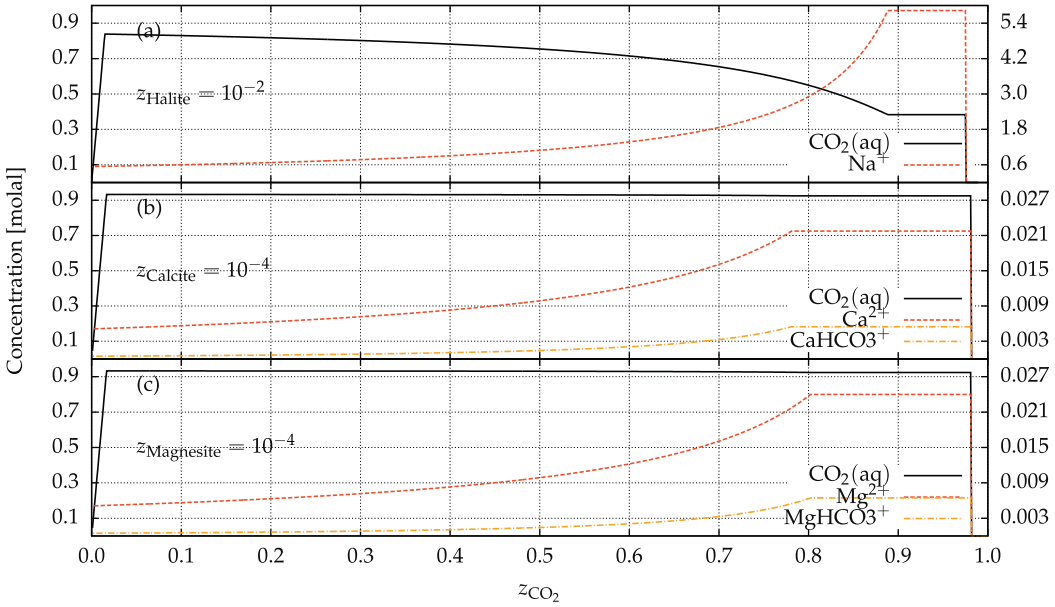

Fig. 11. Phase behaviour of the systems CO_2–H_2O–halite (a), CO_2–H_2O–calcite (b) and CO_2–H_2O–magnesite (c) respectively along the line of feed molar fraction $z_{Halite} = 10^{-2}, z_{Calcite} = 10^{-4}$ and $z_{Magnesite} = 10^{-4}$. Concentrations of CO_2(aq) are given on the left vertical axis and concentrations of other aqueous species on the right. The calculations assumed a CO_2–H_2O–mineral system composed of an aqueous, gaseous and mineral phase.

Table 7
Elemental molar abundance for the equilibrium calculation in the multiphase system CO_2–H_2O–halite–calcite–magnesite.

Element	C	H	O	Na	Cl	Mg	Ca
Moles	0.55	0.84	1.72	0.03	0.03	0.05	0.15

It can be observed from Table 9 that PHREEQC v3.0 [11] fails to accurately estimate the solubility of CO_2 at higher salinities. For 4.0 molal NaCl brines, solubility results obtained using PHREEQC have percentage deviations of 18% in average. At extreme conditions of temperature, pressure and salinity, a percentage deviation error of 26% was achieved with the same solver.

The solubility model of Duan and Sun [38] performed better, even at high temperatures, pressures and salinities. However, the use of our solver with a proper selection of activity and fugacity coefficient models yielded the most accurate solubility results for most of the temperature, pressure and salinity conditions, as seen in Table 9.

Table 8
Chemical equilibrium calculation of the system CO_2–H_2O–halite–calcite–magnesite at $T = 100$ °C and $P = 300$ bar.

Species	Moles	Species	Moles
H_2O	$4.1856 \cdot 10^{-1}$	Mg^{2+}	$4.3106 \cdot 10^{-5}$
$CO_2(g)$	$3.4519 \cdot 10^{-1}$	$CaCl^{+}$	$2.6723 \cdot 10^{-5}$
Calcite	$1.4983 \cdot 10^{-1}$	$CaHCO_3^{+}$	$1.4951 \cdot 10^{-5}$
Magnesite	$4.9887 \cdot 10^{-2}$	$MgHCO_3^{+}$	$1.0122 \cdot 10^{-5}$
Cl^{-}	$2.9808 \cdot 10^{-2}$	H^{+}	$1.0410 \cdot 10^{-7}$
Na^{+}	$2.9754 \cdot 10^{-2}$	HCl(aq)	$4.8159 \cdot 10^{-8}$
$CO_2(aq)$	$4.5251 \cdot 10^{-3}$	$CaCO_3(aq)$	$2.2379 \cdot 10^{-8}$
$H_2O(g)$	$1.1518 \cdot 10^{-3}$	CO_3^{2-}	$1.0799 \cdot 10^{-8}$
HCO_3^{-}	$3.0034 \cdot 10^{-4}$	$MgCO_3(aq)$	$3.6597 \cdot 10^{-9}$
$NaHCO_3(aq)$	$2.4559 \cdot 10^{-4}$	$NaCO_3^{-}$	$2.1094 \cdot 10^{-9}$
Ca^{2+}	$7.7644 \cdot 10^{-5}$	OH^{-}	$2.5126 \cdot 10^{-10}$
$MgCl^{+}$	$6.0074 \cdot 10^{-5}$	NaOH(aq)	$1.2635 \cdot 10^{-10}$
$CaCl_2(aq)$	$5.2820 \cdot 10^{-5}$	Halite	$1.2358 \cdot 10^{-13}$

5. Concluding remarks

A chemical equilibrium method for general multiphase systems has been developed. The method is based on a stoichiometric formulation which solves a system of non-linear mass-action equations coupled with a system of general equilibrium constraint equations. To determine the stable phase assemblage at equilibrium, a stabilisation procedure was developed.

The method was applied to problems relevant to carbon dioxide storage in saline aquifers. A combination of activity and fugacity models were used. The activity coefficient model of Drummond [37] was slightly more accurate than the Duan and Sun [38] model for NaCl brines. However, it was observed that the Duan and Sun [38] model is far superior than the one of Drummond [37] for brines with salt compositions different from NaCl. The fugacity coefficient model of Duan et al. [41] for $CO_2(g)$ was determined

Table 9
Comparison of our calculations of carbon dioxide solubility in NaCl brine with the calculations using PHREEQC v3.0 [10] and the solubility model of Duan and Sun [38] as well as with the experimental solubility data of Hou et al. [30].

T (K)	P (bar)	m_{NaCl}	m_{Exp}	$m_{PHREEQC}$	m_{Duan}	m_{This}	$Error_{PHREEQC}$ (%)	$Error_{Duan}$ (%)	$Error_{This}$ (%)
323.15	27.82	2.5	0.2744	0.2716	0.3016	0.2819	1.038	9.893	2.709
	57.39		0.4900	0.4738	0.5233	0.4951	3.303	6.800	1.038
	87.3		0.6435	0.5986	0.6645	0.6274	6.977	3.264	2.507
	117.73		0.6958	0.6581	0.7229	0.6799	5.419	3.894	2.289
	150.2		0.7271	0.6948	0.7518	0.7096	4.445	3.394	2.409
	182.11		0.7511	0.7237	0.7788	0.7325	3.643	3.694	2.473
						Average	**4.137**	**5.156**	**2.237**
373.15	26.13	2.5	0.1413	0.1424	0.1682	0.1565	0.743	18.996	10.695
	57.42		0.2969	0.2860	0.3324	0.3132	3.665	11.964	5.501
	87.89		0.4133	0.3952	0.4558	0.4312	4.370	10.294	4.352
	118.67		0.5035	0.4814	0.5504	0.5210	4.398	9.305	3.476
	149.21		0.5788	0.5475	0.6198	0.5864	5.410	7.081	1.311
	180.13		0.6395	0.6005	0.6696	0.6360	6.101	4.703	0.555
						Average	**4.115**	**10.391**	**4.315**
423.15	26.43	2.5	0.1073	0.1012	0.1241	0.1288	5.718	15.617	19.962
	57.66		0.2453	0.2267	0.2749	0.2576	7.588	12.060	4.991
	86.00		0.3575	0.3227	0.3904	0.3663	9.744	9.191	2.438
	116.04		0.4612	0.4135	0.4947	0.4640	10.340	7.267	0.615
	148.81		0.5686	0.4991	0.5909	0.5534	12.226	3.919	2.685
	177.94		0.6384	0.5652	0.6635	0.6199	11.464	3.934	2.892
						Average	**9.513**	**8.665**	**5.597**
323.15	29.83	4.0	0.2246	0.2023	0.2506	0.2289	9.930	11.575	1.932
	59.54		0.3851	0.3413	0.4183	0.3882	11.374	8.620	0.812
	89.53		0.4877	0.4266	0.5240	0.4850	12.532	7.438	0.549
	120.17		0.5358	0.4674	0.5658	0.5224	12.762	5.603	2.505
	149.59		0.5590	0.4908	0.5872	0.5428	12.198	5.047	2.892
	179.54		0.5748	0.5101	0.6084	0.5594	11.264	5.836	2.684
						Average	**11.677**	**7.353**	**1.896**
373.15	29.51	4.0	0.1397	0.1121	0.1523	0.1422	19.743	9.038	1.827
	60.68		0.2487	0.2101	0.2792	0.2653	15.512	12.275	6.693
	89.16		0.3463	0.2803	0.3692	0.3528	19.058	6.614	1.891
	120.03		0.4206	0.3407	0.4442	0.4249	18.993	5.615	1.019
	149.24		0.4798	0.3853	0.4973	0.4752	19.698	3.644	0.969
	181.62		0.5233	0.4243	0.5397	0.5170	18.923	3.128	1.204
						Average	**18.655**	**6.719**	**2.267**
423.15	30.93	4.0	0.1085	0.0850	0.1199	0.1236	21.587	10.556	13.937
	58.16		0.2089	0.1606	0.2232	0.2155	23.135	6.826	3.128
	88.57		0.3104	0.2313	0.3210	0.3109	25.471	3.432	0.179
	119.22		0.3964	0.2955	0.4044	0.3920	25.447	2.028	1.109
	149.79		0.4725	0.3510	0.4753	0.4600	25.710	0.598	2.645
	180.79		0.5448	0.4000	0.5367	0.5179	26.583	1.493	4.936
						Average	**24.656**	**4.155**	**4.322**

Note: m_{NaCl} denotes the salinity of the NaCl brine in molality scale. $m_{PHREEQC}$ and m_{Duan} denote the calculated molality of CO_2 using PHREEQC [10] and the solubility model of Duan and Sun [38] respectively. m_{This} denotes the calculated molality of CO_2 using our solver with the activity coefficient model of Drummond [37] for $CO_2(aq)$ and the fugacity coefficient model of Spycher et al. [40] for $CO_2(g)$ and $H_2O(g)$. $Error_{PHREEQC}$, $Error_{Duan}$ and $Error_{This}$ denote respectively the percentage deviation of $m_{PHREEQC}$, m_{Duan} and m_{This} from m_{Exp}.

to be more accurate than the models of Spycher and Reed [39] and Spycher et al. [40].

Comparison of our calculations of CO_2 solubility with the experimental data of Tong et al. [29] and Hou et al. [30] shows that the method is capable of reproducing them with errors of less than 7%. This demonstrates its potential to be integrated in a reactive transport simulator to model carbon dioxide storage in brine aquifers at high temperatures, pressures, and salinities.

Acknowledgements

We gratefully acknowledge funding from the Qatar Carbonates and Carbon Storage Research Centre (QCCSRC), provided jointly by Qatar Petroleum, Shell, and the Qatar Science & Technology Park.

Appendix A. Stoichiometric formulation

According to Smith and Missen [1], chemical equilibrium calculations are performed by using either a stoichiometric or nonstoichiometric formulation. In this section we demonstrate that both formulations are equivalent, though each one requires a different solution technique. The equivalence is shown by transforming the Gibbs energy minimisation problem into a system of non-linear equations that takes into account the stoichiometric relationship among the species.

Resorting to the first and second law of thermodynamics, it is possible to demonstrate that a system undergoing an isobaric and isothermal process tends to a state of equilibrium where its Gibbs free energy is at a global minimum. Assuming that the chemical system of interest is a closed-system, it follows that the law of mass conservation must be applied to its chemical elements. Therefore, combining both these thermodynamic and physical conditions, the equilibrium problem can be formulated as:

$$\min_{\mathbf{n}} G(T,P,\mathbf{n}) \tag{A.1}$$

subject to

$$\sum_{i=1}^{E} w_{ji} n_i = b_j \quad (j=1,\ldots,E), \tag{A.2}$$

where T and P denote, respectively, the temperature and pressure of the system; $\mathbf{n}=[n_1,\ldots,n_N]^t$ the compositional vector of the system; n_i the number of moles of the i-th species; w_{ji} the number of atoms of the j-th element in the i-th species; b_j the molar abundance of the j-th element; and G the Gibbs free energy of the system given by:

$$G=\sum_{i=1}^{N} n_i \mu_i, \tag{A.3}$$

where $\mu_i=\mu_i(T,P,\mathbf{n})$ denotes the chemical potential of the i-th species, which is by definition given by:

$$\mu_i := \left[\frac{\partial G}{\partial n_i}\right]_{T,P,n_{j\neq i}}. \tag{A.4}$$

Eqs. (A.1) and (A.2) constitute a constrained minimisation problem. We remark that besides the equality constrains given by Eq. (A.2), the molar composition of every species is required to be non-negative.

Applying the method of Lagrange multipliers to Eqs. (A.1) and (A.2), the constrained minimisation problem is transformed into an unconstrained one. This is done by defining the Lagrangian function $\mathcal{L}$ as:

$$\mathcal{L}(\mathbf{n},\boldsymbol{\lambda})=\sum_{i=1}^{N} n_i\mu_i+\sum_{j=1}^{E}\lambda_j\left[b_j-\sum_{i=1}^{N} w_{ji}n_i\right], \tag{A.5}$$

where $\boldsymbol{\lambda}=[\lambda_1,\ldots,\lambda_E]^t$ is the vector of Lagrange multipliers. The problem now consists of the minimisation of the Lagrangian $\mathcal{L}$ whose unknowns are $\mathbf{n}$ and $\boldsymbol{\lambda}$.

The solution of the previous unconstrained minimisation problem can be obtained from the first-order necessary conditions for a minimum of $\mathcal{L}$:

$$\frac{\partial \mathcal{L}}{\partial n_i}=\mu_i-\sum_{j=1}^{E} w_{ji}\lambda_j=0 \quad (i=1,\ldots,N), \tag{A.6}$$

$$\frac{\partial \mathcal{L}}{\partial \lambda_j}=b_j-\sum_{i=1}^{N} w_{ji}n_i=0 \quad (j=1,\ldots,E), \tag{A.7}$$

which consists of a system of non-linear algebraic equations in the unknowns $\mathbf{n}$ and $\boldsymbol{\lambda}$.

The stoichiometric formulation can now be derived from Eqs. (A.6) and (A.7). The approach consists of using the stoichiometry among the species in order to eliminate the Lagrange multipliers $\boldsymbol{\lambda}$, reducing therefore the number of unknowns in the problem.

The stoichiometry among the species can be determined by exploring the kernel of the $E\times N$ formula matrix $\mathbf{W}=\{w_{ji}\}$. Assuming that $\mathrm{rank}(\mathbf{W})=E$, it follows from linear algebra that there exists a non-unique set $\{\boldsymbol{\nu}_j\}_{j=1}^{M}$ of $M=N-E$ linearly independent vectors such that:

$$\mathbf{W}\boldsymbol{\nu}_j=\mathbf{0} \quad (j=1,\ldots,M). \tag{A.8}$$

Using the above result, the elimination of the Lagrange multipliers from Eq. (A.6) can now be performed. This is done by writing Eq. (A.6) in matrix form as:

$$\boldsymbol{\mu}-\mathbf{W}^t\boldsymbol{\lambda}=0, \tag{A.9}$$

which after multiplication by $\boldsymbol{\nu}_j^t$ with the simplification given by Eq. (A.8), results in:

$$\boldsymbol{\nu}_j^t\boldsymbol{\mu}=0 \quad (j=1,\ldots,M), \tag{A.10}$$

where $\boldsymbol{\mu}=[\mu_1,\ldots,\mu_N]^t$ is the vector of chemical potentials of the species. Equivalently, we write the stoichiometric transformation of Eq. (A.6) given by (A.10) as:

$$\sum_{i=1}^{N}\nu_{ji}\mu_i=0 \quad (j=1,\ldots,M), \tag{A.11}$$

where ν_{ji} is the stoichiometric coefficient of the i-th species in the j-th stoichiometric vector.

Assume the following functional form for the chemical potential:

$$\mu_i=\mu_i^{\circ}+RT\ln a_i, \tag{A.12}$$

where $\mu_i^{\circ}=\mu_i^{\circ}(T,P)$ is the standard chemical potential of the i-th species; R is the universal gas constant; and $a_i=a_i(T,P,\mathbf{n})$ is the activity of the i-th species. By defining the parameter κ_j as:

$$\kappa_j := \exp\left[-\frac{1}{RT}\sum_{i=1}^{N}\nu_{ji}\mu_i^{\circ}\right], \tag{A.13}$$

Eqs. (A.11) and (A.12) can be combined to:

$$\kappa_j=\prod_{i=1}^{N} a_i^{\nu_{ji}} \quad (j=1,\ldots,M). \tag{A.14}$$

Observe that the stoichiometric coefficients ν_{ji} determined from the kernel of the formula matrix $\mathbf{W}$ allows one to write the system of reactions:

$$0 \rightleftharpoons \sum_{i=1}^{N}\nu_{ji}\alpha_i \quad (j=1,\ldots,M), \tag{A.15}$$

where the following sign convention applies: if ν_{ji} is negative, then α_i is a reactant, otherwise α_i is a product. Thus, it can be seen that Eq. (A.14) is the well-known law of mass-action applied to reaction (A.15) and κ_j is its equilibrium constant.

Therefore, we finalise the stoichiometric formulation by stating that the minimisation of the Gibbs free energy of a multiphase system can be determined by solving the system of non-linear mass-action Eqs. (A.14) and the linear mass-balance Eqs. (A.2).

We remark that the global minimum of the Gibbs free energy is a difficult and expensive problem, and the previous formulation does not prevent a local minimum to be found. Nevertheless, if the initial guess is known to be close to the global minimum of the Gibbs free energy, then chances are that the solution will converge to it.

Appendix B. Thermodynamic models

In this section we present some thermodynamic models for the calculation of the activity and fugacity coefficient models for aqueous, gaseous and mineral species. We show how these coefficients can be used to compute the activities of the species, which is a thermodynamic quantity required to calculate the chemical equilibrium state of a multiphase system.

B.1. Activity coefficients for aqueous species

In this section we present some thermodynamic models for activity coefficients for aqueous species. The activity coefficient γ_i of an aqueous species is assumed in this work to be on a molality scale, so that its activity a_i can be calculated as:

$$a_i = \gamma_i m_i, \tag{B.1}$$

where m_i is the molality of the i-th species given by:

$$m_i = 55.508 \frac{n_i}{n_w}, \tag{B.2}$$

with n_w denoting the number of moles of species $H_2O(l)$.

In what follows, we let I and $\bar{I}$ denote, respectively, the effective and stoichiometric ionic strength of an aqueous solution. These are given by:

$$I = \frac{1}{2}\sum_{j=1}^{N_j} m_j Z_j^2 \tag{B.3}$$

and

$$\bar{I} = \frac{1}{2}\sum_{j=1}^{N_k} m_j^* Z_j^2, \tag{B.4}$$

where N_j and N_k denote the number of ions and aqueous complexes respectively; Z_j the electrical charge of the j-th ion; and m_i^* the stoichiometric molality of the j-th ion, which is given by:

$$m_j^* = \sum_{k=1}^{N_k} \nu_{kj} m_k, \tag{B.5}$$

with ν_{kj} denoting the stoichiometry of the j-th ion in the k-th aqueous complex; and m_k the molality of the k-th aqueous complex. The stoichiometric molality of an ion is the molality this ion would have if all aqueous complexes were completely dissolved in the aqueous solution.

B.1.1. HKF model for ionic species

The activity coefficients of the ionic species are calculated using (see [36, Eq. (298)]):

$$\log \gamma_j = -\frac{A_\gamma Z_j^2 \sqrt{I}}{\Lambda} + \log x_w + [\omega_j^{\mathrm{abs}} b_{\mathrm{NaCl}} + b_{\mathrm{Na^+Cl^-}} - 0.19(|Z_j| - 1)]\bar{I}, \tag{B.6}$$

where x_w denotes the molar fraction of water; and Λ is the Debye–Hückel function defined by:

$$\Lambda = 1 + \mathring{\mathrm{a}} B_\gamma \sqrt{\bar{I}}, \tag{B.7}$$

with $\mathring{\mathrm{a}}$ denoting the ion-size parameter given by Eqs. (124) and (125) of Helgeson et al. [36]:

$$\mathring{\mathrm{a}} = \frac{\sum_k^{N_k}\sum_j^{N_j} \nu_{kj} r_{e,j}}{\sum_k^{N_k}\sum_j^{N_j} \nu_{kj}}.$$

Both the absolute Born coefficient ω_j^{abs} and the effective electrostatic radius $r_{e,j}$ of the j-th ion are given in Table 3 of Helgeson et al. [36].

Table B.1
The activity coefficient parameter A_γ of the HKF model in units of $\mathrm{kg^{1/2}/mol^{1/2}}$ calculated at temperatures 0–500 °C and pressures up to 5000 bar.

T (°C)	P (bar)									
	P_{sat}	250	500	750	1000	1500	2000	3000	4000	5000
0	0.4939	0.4871	0.4810	0.4755	0.4705	0.4617	0.4544	0.4427	0.4337	0.4266
25	0.5114	0.5047	0.4985	0.4928	0.4875	0.4782	0.4701	0.4568	0.4462	0.4375
50	0.5354	0.5281	0.5213	0.5151	0.5094	0.4991	0.4901	0.4750	0.4628	0.4526
75	0.5649	0.5565	0.5488	0.5418	0.5353	0.5236	0.5134	0.4963	0.4824	0.4707
100	0.5996	0.5897	0.5807	0.5725	0.5649	0.5515	0.5398	0.5202	0.5043	0.4910
125	0.6396	0.6276	0.6168	0.6070	0.5981	0.5823	0.5688	0.5463	0.5282	0.5131
150	0.6855	0.6707	0.6573	0.6455	0.6348	0.6161	0.6003	0.5743	0.5536	0.5365
175	0.7383	0.7195	0.7028	0.6881	0.6751	0.6528	0.6341	0.6040	0.5803	0.5609
200	0.7995	0.7753	0.7538	0.7355	0.7194	0.6925	0.6703	0.6352	0.6081	0.5861
225	0.8718	0.8401	0.8117	0.7882	0.7682	0.7353	0.7088	0.6678	0.6367	0.6118
250	0.9596	0.9169	0.8783	0.8476	0.8221	0.7815	0.7498	0.7018	0.6662	0.6381
275	1.0704	1.0111	0.9563	0.9152	0.8823	0.8317	0.7934	0.7372	0.6964	0.6646
300	1.2183	1.1325	1.0500	0.9934	0.9502	0.8865	0.8400	0.7739	0.7272	0.6915
325	1.4357	1.3019	1.1668	1.0856	1.0277	0.9467	0.8900	0.8122	0.7588	0.7186
350	1.8233	1.5767	1.3188	1.1970	1.1175	1.0132	0.9438	0.8521	0.7910	0.7460
375		2.2948	1.5300	1.3350	1.2230	1.0871	1.0019	0.8937	0.8241	0.7737
400			1.8509	1.5114	1.3490	1.1700	1.0648	0.9373	0.8581	0.8019
425			2.3997	1.7439	1.5014	1.2632	1.1333	0.9831	0.8930	0.8305
450			3.3844	2.0579	1.6877	1.3685	1.2078	1.0311	0.9291	0.8597
475			4.7805	2.4810	1.9161	1.4874	1.2889	1.0815	0.9662	0.8895
500			6.0949	3.0235	2.1930	1.6213	1.3770	1.1344	1.0047	0.9202

Table B.2
The activity coefficient parameter B_γ of the HKF model in units of $kg^{1/2}/(mol^{1/2}\cdot cm)$ calculated at temperatures 0–500 °C and pressures up to 5000 bar.

T (°C)	P (bar)									
	P_{sat}	250	500	750	1000	1500	2000	3000	4000	5000
0	0.4939	0.4871	0.4810	0.4755	0.4705	0.4617	0.4544	0.4427	0.4337	0.4266
25	0.5114	0.5047	0.4985	0.4928	0.4875	0.4782	0.4701	0.4568	0.4462	0.4375
50	0.5354	0.5281	0.5213	0.5151	0.5094	0.4991	0.4901	0.4750	0.4628	0.4526
75	0.5649	0.5565	0.5488	0.5418	0.5353	0.5236	0.5134	0.4963	0.4824	0.4707
100	0.5996	0.5897	0.5807	0.5725	0.5649	0.5515	0.5398	0.5202	0.5043	0.4910
125	0.6396	0.6276	0.6168	0.6070	0.5981	0.5823	0.5688	0.5463	0.5282	0.5131
150	0.6855	0.6707	0.6573	0.6455	0.6348	0.6161	0.6003	0.5743	0.5536	0.5365
175	0.7383	0.7195	0.7028	0.6881	0.6751	0.6528	0.6341	0.6040	0.5803	0.5609
200	0.7995	0.7753	0.7538	0.7355	0.7194	0.6925	0.6703	0.6352	0.6081	0.5861
225	0.8718	0.8401	0.8117	0.7882	0.7682	0.7353	0.7088	0.6678	0.6367	0.6118
250	0.9596	0.9169	0.8783	0.8476	0.8221	0.7815	0.7498	0.7018	0.6662	0.6381
275	1.0704	1.0111	0.9563	0.9152	0.8823	0.8317	0.7934	0.7372	0.6964	0.6646
300	1.2183	1.1325	1.0500	0.9934	0.9502	0.8865	0.8400	0.7739	0.7272	0.6915
325	1.4357	1.3019	1.1668	1.0856	1.0277	0.9467	0.8900	0.8122	0.7588	0.7186
350	1.8233	1.5767	1.3188	1.1970	1.1175	1.0132	0.9438	0.8521	0.7910	0.7460
375		2.2948	1.5300	1.3350	1.2230	1.0871	1.0019	0.8937	0.8241	0.7737
400			1.8509	1.5114	1.3490	1.1700	1.0648	0.9373	0.8581	0.8019
425			2.3997	1.7439	1.5014	1.2632	1.1333	0.9831	0.8930	0.8305
450			3.3844	2.0579	1.6877	1.3685	1.2078	1.0311	0.9291	0.8597
475			4.7805	2.4810	1.9161	1.4874	1.2889	1.0815	0.9662	0.8895
500			6.0949	3.0235	2.1930	1.6213	1.3770	1.1344	1.0047	0.9202

Note: The values of B_γ were multiplied by 10^{-8}.

Table B.3
The activity coefficient parameter b_{NaCl} of the HKF model in units of kg/cal calculated at temperatures 0–500 °C and pressures up to 5000 bar.

T (°C)	P (bar)									
	P_{sat}	250	500	750	1000	1500	2000	3000	4000	5000
0	21.962	22.211	22.437	22.643	22.831	23.162	23.444	23.901	24.258	24.548
25	18.081	18.321	18.542	18.746	18.934	19.273	19.569	20.063	20.461	20.792
50	14.530	14.783	15.016	15.232	15.432	15.794	16.112	16.648	17.088	17.458
75	11.235	11.516	11.775	12.012	12.233	12.630	12.979	13.570	14.055	14.465
100	8.125	8.449	8.745	9.015	9.264	9.710	10.100	10.757	11.295	11.749
125	5.138	5.521	5.868	6.183	6.470	6.980	7.421	8.158	8.757	9.260
150	2.214	2.678	3.095	3.467	3.804	4.395	4.900	5.733	6.402	6.960
175	−0.710	−0.137	0.376	0.826	1.227	1.919	2.503	3.449	4.200	4.821
200	−3.703	−2.981	−2.336	−1.783	−1.298	−0.477	0.201	1.283	2.127	2.817
225	−6.858	−5.930	−5.096	−4.402	−3.807	−2.824	−2.028	−0.787	0.164	0.932
250	−10.304	−9.082	−7.969	−7.080	−6.339	−5.147	−4.209	−2.779	−1.707	−0.852
275	−14.247	−12.590	−11.042	−9.873	−8.934	−7.476	−6.362	−4.709	−3.498	−2.547
300	−19.060	−16.716	−14.437	−12.856	−11.643	−9.837	−8.506	−6.592	−5.223	−4.166
325	−25.556	−21.993	−18.343	−16.122	−14.524	−12.262	−10.663	−8.439	−6.893	−5.718
350	−36.227	−29.865	−23.076	−19.806	−17.650	−14.783	−12.853	−10.265	−8.519	−7.214
375		−48.639	−29.220	−24.100	−21.113	−17.436	−15.095	−12.080	−10.108	−8.663
400			−38.002	−29.287	−25.032	−20.261	−17.410	−13.895	−11.671	−10.072
425			−52.214	−35.791	−29.554	−23.299	−19.818	−15.719	−13.214	−11.449
450			−76.652	−44.209	−34.857	−26.594	−22.338	−17.561	−14.746	−12.801
475			−110.794	−55.166	−41.133	−30.187	−24.986	−19.429	−16.271	−14.134
500			−143.763	−68.878	−48.527	−34.113	−27.778	−21.329	−17.796	−15.455

Note: The values of b_{NaCl} were multiplied by 10^7.

The parameters $A_\gamma, B_\gamma, b_{NaCl}$ and $b_{Na^+Cl^-}$ have been calculated using equations and parameters from [33–36]. Tables B.1,B.2,B.3,B.4 present the results of this calculation over a wide range of temperatures and pressures. These tables are used in our code to interpolate those parameters at a given temperature and pressure.

The extended Debye–Hückel Eq. (B.6) is valid at temperatures and pressures up to 600 °C and 5000 bar. The use of the stoichiometric ionic strength $\bar{I}$ instead of the effective ionic strength I has been determined to yield more accurate activity coefficients at NaCl brine salinities up to ~6 molal.

B.1.2. HKF model for water

Helgeson et al. [36] derived an equation for the activity of water a_w, which we present in the following form:

$$\ln a_w = \frac{2.303}{55.508}\sum_{j=1}^{N_j} m_j^* \psi_j, \tag{B.8}$$

where

$$\psi_j = \frac{A_\gamma Z_j^2 \sqrt{\bar{I}}}{3}\sigma + \frac{x_w}{1-x_w}\log x_w - \frac{1}{2}[\omega_j b_{NaCl} + b_{Na^+Cl^-} - 0.19(|Z_j|-1)]\bar{I} \tag{B.9}$$

and

$$\sigma = \frac{3}{(\mathring{a}B_\gamma\sqrt{\bar{I}})^3}\left(\Lambda - \frac{1}{\Lambda} - 2\ln\Lambda\right). \tag{B.10}$$

The above activity model is also valid at temperatures, pressures and brine salinities up to 600 °C, 5000 bar and 6 molal.

Table B.4
The activity coefficient parameter $b_{Na^+Cl^-}$ of the HKF model in units of kg/mol calculated at temperatures 0–500 °C and pressures up to 5000 bar.

T (°C)	P (bar)									
	P_{sat}	250	500	750	1000	1500	2000	3000	4000	5000
0	−15.448	−14.872	−14.390	−14.002	−13.708	−13.401	−13.471	−14.739	−17.512	−21.789
25	−9.752	−9.563	−9.404	−9.276	−9.178	−9.073	−9.090	−9.487	−10.370	−11.739
50	−5.630	−5.603	−5.579	−5.560	−5.544	−5.524	−5.518	−5.552	−5.647	−5.801
75	−2.411	−2.466	−2.510	−2.546	−2.571	−2.594	−2.577	−2.430	−2.128	−1.672
100	0.244	0.145	0.063	−0.002	−0.051	−0.097	−0.075	0.172	0.691	1.482
125	2.529	2.405	2.301	2.218	2.156	2.097	2.122	2.426	3.069	4.052
150	4.559	4.421	4.305	4.212	4.142	4.074	4.101	4.438	5.153	6.246
175	6.406	6.263	6.139	6.040	5.966	5.894	5.921	6.276	7.032	8.187
200	8.119	7.976	7.848	7.746	7.670	7.595	7.623	7.987	8.763	9.950
225	9.729	9.591	9.462	9.359	9.282	9.205	9.233	9.600	10.384	11.583
250	11.259	11.130	11.001	10.897	10.820	10.743	10.771	11.138	11.921	13.119
275	12.723	12.608	12.479	12.377	12.300	12.224	12.251	12.614	13.391	14.581
300	14.133	14.036	13.909	13.807	13.731	13.656	13.682	14.041	14.808	15.984
325	15.496	15.421	15.296	15.196	15.121	15.047	15.073	15.426	16.182	17.339
350	16.818	16.771	16.648	16.550	16.476	16.403	16.428	16.775	17.517	18.654
375		18.090	17.969	17.872	17.800	17.728	17.753	18.093	18.821	19.935
400		19.380	19.262	19.167	19.096	19.026	19.050	19.383	20.096	21.188
425		20.645	20.529	20.437	20.367	20.298	20.322	20.648	21.346	22.415
450		21.887	21.774	21.683	21.615	21.547	21.570	21.890	22.572	23.618
475		23.108	22.997	22.908	22.841	22.775	22.798	23.110	23.777	24.801
500		24.308	24.199	24.113	24.048	23.983	24.005	24.310	24.963	25.964

Note: The values of $b_{Na^+Cl^-}$ were multiplied by 10^2.

The parameters $A_\gamma, B_\gamma, b_{NaCl}$ and $b_{Na^+Cl^-}$ are interpolated from Tables B.1,B.2,B.3,B.4.

B.1.3. Setschenow model for neutral species

The activity coefficients for neutral species are calculated using the Setschenow model equation:

$$\log \gamma_i = b_i I + \log x_w, \tag{B.11}$$

where b_i is the Setschenow coefficient of the i-th species. The value $b_i = 0.1$ is adopted in this work for those neutral species whose Setschenow coefficient is not known.

B.1.4. Drummond [37] model for CO_2(aq)

Drummond [37] derived the following equation for the activity coefficient of CO_2(aq):

$$\ln \gamma_{CO_2} = \left(a_1 + a_2 T + \frac{a_3}{T}\right) I - (a_4 + a_5 T)\frac{I}{I+1}, \tag{B.12}$$

where $a_1 = -1.0312, a_2 = 1.2806 \cdot 10^{-3}, a_3 = 255.9, a_4 = 0.4445$ and $a_5 = -1.606 \cdot 10^{-3}$; and T is temperature in units of Kelvin. This equation is valid within the temperature and salinity ranges 20–400 °C and 0–6.5 molal respectively.

B.1.5. Duan and Sun [38] model for CO_2(aq)

Duan and Sun [38] presents the following activity coefficient model for CO_2(aq):

$$\begin{aligned}\ln \gamma_{CO_2} =& 2\lambda(m_{Na^+} + m_{K^+} + 2m_{Ca^{2+}} + 2m_{Mg^{2+}}) \\ &+ \zeta(m_{Na^+} + m_{K^+} + m_{Ca^{2+}} + m_{Mg^{2+}})m_{Cl^-} - 0.07 m_{SO_4^{2-}}\end{aligned} \tag{B.13}$$

where

$$\begin{aligned}\lambda =& -0.411370585 + 6.07632013 \cdot 10^{-4} T + 97.5347708/T \\ &- 0.0237622469 P/T + 0.0170656236 P/(630 - T) \\ &+ 1.41335834 \cdot 10^{-5} T \ln P\end{aligned} \tag{B.14}$$

and

$$\begin{aligned}\zeta =& 3.36389723 \cdot 10^{-4} - 1.98298980 \cdot 10^{-5} T \\ &+ 2.12220830 \cdot 10^{-3} P/T - 5.24873303 \cdot 10^{-3} P/(630 - T),\end{aligned} \tag{B.15}$$

with temperature T and pressure P given in units of Kelvin and bar respectively.

These equations are valid within the temperature, pressure and salinity ranges of 0–260 °C, 0–2000 bar, and 0–4.3 molal. Nevertheless, its use at higher salinities (e.g. up to ~6 molal NaCl and up to ~4 molal $CaCl_2$) yields satisfactory results and this has been done before in [49].

B.1.6. Rumpf et al. [50] model for CO_2(aq)

Based on a Pitzer formulation with correlation of solubility data, Rumpf et al. [50] derived the following activity coefficient model for CO_2(aq) (see [49]):

$$\begin{aligned}\ln \gamma_{CO_2} =& 2B(m_{Na^+} + m_{K^+} + 2m_{Ca^{2+}} + 2m_{Mg^{2+}}) \\ &+ 3\Gamma(m_{Na^+} + m_{K^+} + m_{Ca^{2+}} + m_{Mg^{2+}})m_{Cl^-}\end{aligned} \tag{B.16}$$

where $\Gamma = -0.0028$ and

$$B = 0.254 - \frac{76.82}{T} - \frac{10656}{T^2} + \frac{6312 \cdot 10^3}{T^3}, \tag{B.17}$$

with temperature T given in units of Kelvin.

These equations are valid within the temperature range of 40–160 °C, at brine salinities up to ~6 molal NaCl and at pressures up to 100 bar. Therefore, this model is unsuitable for CO_2 solubility modelling at high pressures, though it is accurate enough within its valid temperature and pressure ranges.

B.2. Fugacity coefficients for gaseous species

In this section we present some thermodynamic models for fugacity coefficients for gaseous species. The fugacity coefficient φ_i of a gaseous species is used to calculate its activity a_i as:

$$a_i = \varphi_i y_i \frac{P}{P^\circ}, \tag{B.18}$$

where y_i is the molar fraction of the i-th gaseous species in the gaseous phase; and $P^\circ = 1$ bar is the standard pressure assumed in this work.

Table B.5
Coefficients from Table 1 of Spycher and Reed [39] for the calculation of fugacity coefficients of pure gases.

Gas	T (°C)	P_{max} (bar)	a	b	c ($\times10^5$)	d ($\times10^2$)	e ($\times10^5$)	f ($\times10^8$)
H_2	25–600	3000	−12.5908	0.259789	−7.24730	0.471947	−2.69962	2.15622
H_2O	0–1000	1000	−3238.36	4.69231	−175.120	272.189	−463.667	202.904
	0–340	P_{sat}	−6191.41	14.8528	−914.267	−6633.26	18277.0	−13274.0
CO_2	400–1000	1000	−361.447	0.553372	−0.549789	16.3871	3.86767	−9.26594
	50–350	500	−1430.87	3.59800	−227.376	347.644	−1042.47	846.271
CH_4	16–350	500	−537.779	1.54946	−92.7827	120.861	−370.814	333.804

Table B.6
Cross-coefficients from Table 2 of Spycher and Reed [39] for the calculation of fugacity coefficients of mixed gases.

Mixture (ij)	T (°C)	P_{max} (bar)	a_{ij}	b_{ij}	c_{ij} ($\times10^2$)	d_{iij}	e_{iij} ($\times10^2$)	f_{iij} ($\times10^5$)	d_{ijj}	e_{ijj} ($\times10^2$)	f_{ijj} ($\times10^5$)
H_2O–CO_2	450–1000	1000	−1286.47	2.95028	−0.165412	2.54908	−0.494212	0.239023	0.0	0.0	0.0
	50–350	500	−1954.70	7.74805	−1.029010	104.453	−38.42830	36.58580	−8.28426	1.19097	0.808886
H_2O–CH_4	25–100	94	−1103.20	4.52871	−0.507784	0.0	0.0	0.0	0.0	0.0	0.0
CO_2–CH_4	40–240	500	−800.592	2.28990	−0.153917	2.99160	−1.04893	1.02627	1.58384	−0.492077	0.430104

Note: For H_2O–CO_2 mixtures, the coefficients of this table for the temperature range 50–350 °C must be used only with the coefficients for the range 0–340 °C in Table B.5.

B.2.1. Spycher and Reed [39] model for $H_2O(g)$–$CO_2(g)$–$CH_4(g)$

Spycher and Reed [39] derived fugacity coefficient equations for pure and mixed gases based on a virial expansion formulation. In this work we opted to use the equations of Spycher and Reed [39] where the gaseous phase is assumed as a non-ideal mixture of gases because of its reliability and accuracy at pressures higher than the saturation pressure of water.

In what follows, we denote 1-H_2O(g), 2-CO_2(g) and 3-CH_4(g). The fugacity coefficients of the end-members of the gaseous mixture H_2O–CO_2–CH_4, therefore, are given by:

$$\ln\varphi_i = \left[2\sum_{k=1}^{3}\hat{y}_k B'_{ik} - B'_{\text{mix}}\right]P + \left[\frac{3}{2}\sum_{k=1}^{3}\sum_{l=1}^{3}\hat{y}_k\hat{y}_l C'_{ikl} - C'_{\text{mix}}\right]P^2, \tag{B.19}$$

where $\hat{y}_k$ denotes the molar fraction of the k-th gas in the mixture H_2O–CO_2–CH_4. This is in contrast with y_k, which represents the molar fraction of the k-th gas in the gaseous phase, which may contain other additional gases (e.g., O_2(g), H_2(g)). The second and third cross-virial coefficients B'_{ij} and C'_{ijk} are calculated using:

$$B'_{ij} = \frac{a_{ij}}{T^2} + \frac{b_{ij}}{T} + c_{ij}, \tag{B.20}$$

$$C'_{ijk} = \frac{d_{ijk}}{T^2} + \frac{e_{ijk}}{T} + f_{ijk}, \tag{B.21}$$

where

$$B'_{\text{mix}} = \sum_{i=1}^{3}\sum_{k=1}^{3}\hat{y}_i\hat{y}_k B'_{ik}, \tag{B.22}$$

$$C'_{\text{mix}} = \sum_{i=1}^{3}\sum_{k=1}^{3}\sum_{l=1}^{3}\hat{y}_i\hat{y}_k\hat{y}_l C'_{ikl}. \tag{B.23}$$

The parameters $a_{ij}, b_{ij}, c_{ij}, d_{ijk}, e_{ijk}$ and f_{ijk} are presented in Tables B.5 and B.6. Note that temperature T and pressure P are given in units of Kelvin and bar respectively.

B.2.2. Spycher et al. [40] model for $H_2O(g)$–$CO_2(g)$

From a modified Redlich–Kwong equation of state, Spycher et al. [40] derived the following fugacity coefficient equations for the gaseous species H_2O(g) and CO_2(g):

$$\ln\phi_{H_2O} = \ln\left(\frac{v}{v-b_m}\right) + \left(\frac{b_{H_2O}}{v-b_m}\right) + \frac{a_m b_{H_2O}}{RT^{1.5}b_m}\left[\ln\left(\frac{v+b_{H_2O}}{v}\right) - \frac{b_m}{v+b_m}\right] - \frac{2a_{CO_2-H_2O}}{RT^{0.5}b_m}\ln\left(\frac{v+b_m}{v}\right) - \ln\left(\frac{Pv}{RT}\right), \tag{B.24}$$

and

$$\ln\phi_{CO_2} = \ln\left(\frac{v}{v-b_m}\right) + \left(\frac{b_{CO_2}}{v-b_m}\right) + \frac{a_m b_{CO_2}}{RT^{1.5}b_m}\left[\ln\left(\frac{v+b_{CO_2}}{v}\right) - \frac{b_m}{v+b_m}\right] - \frac{2a_{CO_2}}{RT^{0.5}b_m}\ln\left(\frac{v+b_m}{v}\right) - \ln\left(\frac{Pv}{RT}\right), \tag{B.25}$$

where v is the molar volume of the mixture, in units of cm^3/mol, given by the solution of the cubic equation:

$$v^3 - v^2\left(\frac{RT}{P}\right) - v\left(\frac{RTb_m}{P} - \frac{a_m}{PT^{0.5}} + b_m^2\right) - \frac{a_m b_m}{PT^{0.5}} = 0 \tag{B.26}$$

with temperature T and pressure P given in units of Kelvin and bar respectively. The parameters from the previous equations are shown in Table B.7. These equations are valid at temperatures 12–100 °C and pressures up to 600 bar.

Note that Spycher et al. [40] assumed that $\hat{y}_{CO_2} = 1$ and $\hat{y}_{H_2O} = 0$ to derive Eqs. (B.24) and (B.25). This simplification results in $a_m = a_{CO_2}$ and $b_m = b_{CO_2}$.

B.2.3. Duan et al. [41] model for $CO_2(g)$

Duan et al. [41] presents an improved fugacity coefficient equation for CO_2(g), which can be calculated efficiently and directly as

Table B.7
The parameters for Eqs. (B.24) and (B.25) taken from [40].

Parameter	Value	Unit
b_{H_2O}	18.18	cm^3/mol
b_{CO_2}	27.8	cm^3/mol
$a_{CO_2-H_2O}$	$7.89\cdot10^7$	bar·cm^6·K$^{0.5}$/mol^2
a_{CO_2}	$7.54\cdot10^7 - 4.13\cdot10^4 T$	bar·cm^6·K$^{0.5}$/mol^2

Table B.8
The parameters for the fugacity coefficient model of Duan et al. [41] for CO_2(g).

Parameter	T–P range					
	1	2	3	4	5	6
c_1	1	−7.1734882E−1	−6.5129019E−2	5.0383896E+0	−1.6063152E+1	−1.5693490E−1
c_2	4.7586835E−3	1.5985379E−4	−2.1429977E−4	−4.4257744E−3	−2.7057990E−3	4.4621407E−4
c_3	−3.3569963E−6	−4.9286471E−7	−1.1444930E−6	0	0	−9.1080591E−7
c_4	0	0	0	1.9572733E+0	1.4119239E−1	0
c_5	−1.3179396E+0	0	0	0	0	0
c_6	−3.8389101E−6	−2.7855285E−7	−1.1558081E−7	2.4223436E−6	8.1132965E−7	1.0647399E−7
c_7	0	1.1877015E−9	1.1952370E−9	0	0	2.4273357E−10
c_8	2.2815104E−3	0	0	−9.3796135E−4	−1.1453082E−4	0
c_9	0	0	0	−1.5026030E+0	2.3895671E+0	3.5874255E−1
c_{10}	0	0	0	3.0272240E−3	5.0527457E−4	6.3319710E−5
c_{11}	0	0	0	−3.1377342E+1	−1.7763460E+1	−2.4989661E+2
c_{12}	0	−9.6539512E+1	−2.2134306E+2	−1.2847063E+1	9.8592232E+2	0
c_{13}	0	4.4774938E−1	0	0	0	0
c_{14}	0	1.0181078E+2	7.1820393E+1	0	0	8.8876800E+2
c_{15}	0	5.3783879E−6	6.6089246E−6	−1.5056648E−5	−5.4965256E−7	−6.6348003E−7

Range 1: 273 K < T < 573 K, $P < P^*$; range 2: 273 K < T < 340 K, $P^* < P$ < 1000 bar; range 3: 273 K < T < 340 K, P > 1000 bar; range 4: 340 K < T < 435 K, $P^* < P$ < 1000 bar; range 5: 340 K < T < 435 K, P > 1000 bar; range 6: T > 435 K, $P > P^*$.

opposed to the costly and iterative scheme required in [38]. The fugacity coefficient equation is given by:

$$\varphi_{CO_2} = c_1 + [c_2 + c_3T + c_4/T + c_5/(T-150)]P + (c_6 + c_7T + c_8/T)P^2 + (c_9 + c_{10}T + c_{11}/T)\ln P + (c_{12} + c_{13}T)/P + c_{14}/T + c_{15}T^2, \quad (B.27)$$

where temperature T and pressure P are given in units of Kelvin and bar respectively; and the parameters c_1 through c_{15} are given in Table B.8. This equation is valid at temperatures 0–260 °C and pressures up to 2000 bar.

In Table B.8, the auxiliary pressure P^*, in units of bar, is calculated using:

$$P^* = \begin{cases} P^{sat}_{CO_2} & T < 305\ \text{K} \\ 75 + 1.25(T-305) & 305\ \text{K} < T < 405\ \text{K} \\ 200 & T > 405\ \text{K} \end{cases}, \quad (B.28)$$

where $P^{sat}_{CO_2}$ is the saturation pressure of CO_2, which can be computed using the equation of state developed by Poling et al. [51]:

$$\ln\left(\frac{P^{sat}_{CO_2}}{P^{cr}_{CO_2}}\right) = \frac{a_1x + a_2x^{1.5} + a_3x^3 + a_4x^6}{1-x}, \quad (B.29)$$

with $a_1 = -6.95626, a_2 = 1.19695, a_3 = -3.12614, a_4 = 2.99448$ and $x = 1 - T/T^{cr}_{CO_2}$, where $T^{cr}_{CO_2} = 304.2$ K and $P^{cr}_{CO_2} = 73.83$ bar are the critical temperature and pressure of CO_2 respectively.

B.3. Activity coefficients for mineral species

In this work the ideal model for the activity coefficients of mineral species is assumed. Therefore, the activity a_i of the i-th mineral in a mineral solution is given by:

$$a_i = x_i, \quad (B.30)$$

from which it follows that $a_i = 1$ for pure minerals.

References

[1] Smith WR, Missen RW. Chemical reaction equilibrium analysis: theory and algorithms. New York: Wiley; 1982.
[2] Zeleznik FJ, Gordon S. Calculation of complex chemical equilibria. Ind Eng Chem 1968;60:27–57.
[3] Van Zeggeren F, Storey SH. The computation of chemical equilibria. London, England: Cambridge University Press; 1970.
[4] Westall J, Zachary J, Morel F. MINEQL: a computer program for the calculation of chemical equilibrium composition of aqueous systems. 1976.
[5] Schecher W, McAvoy D. MINEQL+: A chemical equilibrium modeling system. Hallowell: Environmental Research Software; 1998.
[6] Truesdell A, Jones B. WATEQ–A computer program for calculating chemical equilibrium of natural waters. J Res US Geol Surv 1974;2(2):233–48.
[7] Ball J, Nordstrom D. WATEQ4F – a personal computer FORTRAN translation of the geochemical model WATEQ2 with revised data base. US Geol Sur Open-File Rep 1987;87(50):108.
[8] Allison J, Kevin J. MINTEQA2/PRODEFA2: a geochemical assessment model for environmental systems: version 3.0 user's manual. US Environmental Protection Agency, Report EPA(600/3-91/021), 1991.
[9] Wolery TJ. EQ3/6, a software package for geochemical modeling of aqueous systems: package overview and installation guide (version 7.0). 1992.
[10] Parkhurst D, Appelo C. User's guide to PHREEQC (version 2) – a computer program for speciation, batch-reaction, one-dimensional transport, and inverse geochemical calculations. Water Resour Invest Rep US Geol Surv 1999;99(4259):326.
[11] Parkhurst D, Appelo C. Description of input and examples for PHREEQC version 3 – a computer program for speciation, batch-reaction, one-dimensional transport, and inverse geochemical calculations. In: Groundwater book 6, modeling techniques; U.S. geological survey techniques and methods, 2013. p. 497 [chapter A43]. URL http://pubs.usgs.gov/tm/06/a43.
[12] van der Lee J, Windt LD. CHESS tutorial and cookbook, version 3.0. Technical Report 1-2, Ecole des Mines de Paris, Fontainebleau, France, 2002.
[13] Bethke CM. Geochemical and biogeochemical reaction modeling. 2nd ed. Cambridge University Press; 2007. ISBN 0521875544.
[14] Kulik D, Berner U, Curti E. Modelling chemical equilibrium partitioning with the GEMS-PSI code. PSI Sci Rep 2004;IV:109–22.
[15] Bale C, Chartrand P, Degterov S, Eriksson G, Hack K, Ben Mahfoud R, et al. FactSage thermochemical software and databases. Calphad 2002;26(2):189–228. http://dx.doi.org/10.1016/S0364-5916(02)00035-4.
[16] Bale C, Bélisle E, Chartrand P, Decterov S, Eriksson G, Hack K, et al. FactSage thermochemical software and databases – recent developments. Calphad 2009;33(2):295–311. http://dx.doi.org/10.1016/j.calphad.2008.09.009.
[17] Eriksson G, Hack K. ChemSage – a computer program for the calculation of complex chemical equilibria. Metall Mater Trans B 1990;21(6):1013–23. http://dx.doi.org/10.1007/BF02670272.
[18] Wolery TJ, Daveler SA. EQ6, a computer program for reaction path modeling of aqueous geochemical systems: theoretical manual, user's guide, and related documentation (version 7.0). 1992.
[19] Wolery TJ. EQ3NR, a computer program for geochemical squeous speciation-solubility calculations: theoretical manual, user's guide, and related documentation (version 7.0). 1992.
[20] Morel F, Morgan J. Numerical method for computing equilibriums in aqueous chemical systems. Environ Sci Technol 1972;6(1):58–67. http://dx.doi.org/10.1021/es60060a006.
[21] Reed MH. Calculation of multicomponent chemical equilibria and reaction processes in systems involving minerals, gases and an aqueous phase. Geochim Cosmochim Acta 1982;46(4):513–28. http://dx.doi.org/10.1016/0016-7037(82)90155-7.
[22] Perez R, Heidemann R, Perez E. A new approach to multiphase geochemical speciation modeling. Appl Geochem 2012;27(9):1724–37. http://dx.doi.org/10.1016/j.apgeochem.2012.02.008.
[23] Johnson J, Nitao J, Knauss K. Reactive transport modelling of CO2 storage in saline aquifers to elucidate fundamental processes, trapping mechanisms and sequestration partitioning. Geol Soc London Spec Publ 2004;233(1):107.

[24] Lagneau V, Pipart A, Catalette H. Reactive transport modelling of CO2 sequestration in deep saline aquifers. Oil Gas Sci Technol 2005;60(2):231–48.
[25] Audigane P, Gaus I, Pruess K, Xu T. Reactive transport modeling using TOUGHREACT for the long term CO2 storage at Sleipner, North Sea. In: 4th Annual Conference on Carbon Capture and Sequestration DOE/NETL, 2005.
[26] Audigane P, Gaus I, Czernichowski-Lauriol I, Pruess K, Xu T. Two-dimensional reactive transport modeling of CO2 injection in a saline aquifer at the Sleipner site, North Sea. Am J Sci 2007;307(7):974–1008. http://dx.doi.org/10.2475/07.2007.02.
[27] Fan Y, Durlofsky LJ, Tchelepi Ha. A fully-coupled flow-reactive-transport formulation based on element conservation, with application to CO2 storage simulations. Adv Water Resour 2012;42:47–61. http://dx.doi.org/10.1016/j.advwatres.2012.03.012.
[28] Gunter WD, Wiwehar B, Perkins EH. Aquifer disposal of CO2-rich greenhouse gases: extension of the time scale of experiment for CO2-sequestering reactions by geochemical modelling. Miner Petrol 1997;59(1-2):121–40. http://dx.doi.org/10.1007/BF01163065.
[29] Tong D, Trusler JPM, Vega-Maza D. Solubility of CO2 in aqueous solutions of MgCl2 or CaCl2 and in a synthetic formation brine at temperatures up to 423 K and pressures up to 40 MPa, in preparation.
[30] Hou SX, Maitland G, Trusler JPM. Phase Equilibria of (CO2 + H2O + NaCl) and (CO2 + H2O + KCl): measurements and modeling. J Supercritic Fluids, submitted for publication. CO2 + KCl + H2O mixtures: measurements and modeling, submitted for publication.
[31] Anderson GM, Crerar DA. Thermodynamics in geochemistry: the equilibrium model. New York: Oxford University Press; 1993. ISBN 019506464X.
[32] Whitson C, Michelsen M. The negative flash. Fluid Phase Equilib 1989;53(2):51–71. Available from: http://linkinghub.elsevier.com/retrieve/pii/037838128980072X.
[33] Helgeson HC, Kirkham DH. Theoretical prediction of the thermodynamic behavior of aqueous electrolytes at high pressures and temperatures: I. Summary of the thermodynamic/electrostatic properties of the solvent. Am J Sci 1974;274(10):1089–198. http://dx.doi.org/10.2475/ajs.274.10.1089.
[34] Helgeson HC, Kirkham DH. Theoretical prediction of the thermodynamic behavior of aqueous electrolytes at high pressures and temperatures: II. Debye–Huckel parameters for activity coefficients and relative partial molal properties. Am J Sci 1974;274(10):1199–261. http://dx.doi.org/10.2475/ajs.274.10.1199.
[35] Helgeson HC, Kirkham DH. Theoretical prediction of the thermodynamic properties of aqueous electrolytes at high pressures and temperatures: III. Equation of state for aqueous species at infinite dilution. Am J Sci 1976;276(2):97–240. http://dx.doi.org/10.2475/ajs.276.2.97.
[36] Helgeson HC, Kirkham DH, Flowers GC. Theoretical prediction of the thermodynamic behavior of aqueous electrolytes by high pressures and temperatures: IV. Calculation of activity coefficients, osmotic coefficients, and apparent molal and standard and relative partial molal properties to 600 °C. Am J Sci 1981;281(10):1249–516. http://dx.doi.org/10.2475/ajs.281.10.1249.
[37] Drummond S. Boiling and mixing of hydrothermal fluids: chemical effects on mineral precipitation. PhD, Pennsylvania State University, 1981.
[38] Duan Z, Sun R. An improved model calculating CO2 solubility in pure water and aqueous NaCl solutions from 273 to 533 K and from 0 to 2000 bar. Chem Geol 2003;193(3–4):257–71. http://dx.doi.org/10.1016/S0009-2541(02)00263-2.
[39] Spycher N, Reed M. Fugacity coefficients of H2, CO2, CH4, H2O and of H2O–CO2–CH4 mixtures: a virial equation treatment for moderate pressures and temperatures applicable to calculations of hydrothermal boiling. Geochim Cosmochim Acta 1988;52(3):739–49. http://dx.doi.org/10.1016/0016-7037(88)90334-1.
[40] Spycher N, Pruess K, Ennis-King J. CO2–H2O mixtures in the geological sequestration of CO2. I. Assessment and calculation of mutual solubilities from 12 to 100 °C and up to 600 bar. Geochim Cosmochim Acta 2003;67(16):3015–31. http://dx.doi.org/10.1016/S0016-7037(03)00273-4.
[41] Duan Z, Sun R, Zhu C, Chou IM. An improved model for the calculation of CO2 solubility in aqueous solutions containing Na^+, K^+, Ca^{2+}, Mg^{2+}, Cl^-, and SO_4^{2-}. Mar Chem 2006;98(2-4):131–9. http://dx.doi.org/10.1016/j.marchem.2005.09.001.
[42] Duan Z, Møller N, Weare JH. An equation of state for the CH4–CO2–H2O system: I. Pure systems from 0 to 1000 °C and 0 to 8000 bar. Geochim Cosmochim Acta 1992;56(7):2605–17. http://dx.doi.org/10.1016/0016-7037(92)90347-L.
[43] Helgeson H, Delany J, Nesbitt H, Bird D. Summary and critique of the thermodynamic properties of rock-forming minerals. Am J Sci 1978;278A(1).
[44] Tanger JC, Helgeson HC. Calculation of the thermodynamic and transport properties of aqueous species at high pressures and temperatures; revised equations of state for the standard partial molal properties of ions and electrolytes. Am J Sci 1988;288(1):19–98. http://dx.doi.org/10.2475/ajs.288.1.19.
[45] Shock E, Helgeson HC. Calculation of the thermodynamic and transport properties of aqueous species at high pressures and temperatures: correlation algorithms for ionic species and equation of state predictions to 5 kb and 1000 °C. Geochim Cosmochim Acta 1988;52(8):2009–36. http://dx.doi.org/10.1016/0016-7037(88)90181-0.
[46] Shock EL, Oelkers EH, Johnson JW, Sverjensky DA, Helgeson HC. Calculation of the thermodynamic properties of aqueous species at high pressures and temperatures. Effective electrostatic radii, dissociation constants and standard partial molal properties to 1000 °C and 5 kbar. J Chem Soc Faraday T 1992;88(6):803. http://dx.doi.org/10.1039/ft9928800803.
[47] Johnson JW, Oelkers EH, Helgeson HC. SUPCRT92: a software package for calculating the standard molal thermodynamic properties of minerals, gases, aqueous species, and reactions from 1 to 5000 bar and 0 to 1000 °C. Comput Geosci 1992;18(7):899–947. http://dx.doi.org/10.1016/0098-3004(92)90029-Q.
[48] Wagner W, Pruss A. The IAPWS formulation 1995 for the thermodynamic properties of ordinary water substance for general and scientific use. J Phys Chem Ref Data 2002;31(2):387–444. http://dx.doi.org/10.1063/1.1461829.
[49] Spycher N, Pruess K. CO2–H2O mixtures in the geological sequestration of CO2. II. Partitioning in chloride brines at 12–100 °C and up to 600 bar. Geochim Cosmochim Acta 2005;69(13):3309–20. http://dx.doi.org/10.1016/j.gca.2005.01.015.
[50] Rumpf B, Nicolaisen H, Ocal C, Maurer G. Solubility of carbon dioxide in aqueous solutions of sodium chloride: experimental results and correlation. J Solution Chem 1994;23(3):431–48. http://dx.doi.org/10.1007/BF00973113.
[51] Poling BE, Prausnitz JM, O'Connell JP. The properties of gases and liquids. McGraw-Hill; 2001.